SOURCE DATA   TRANSPARENT PROCESS   OPEN ACCESS

THE EMBO JOURNAL

A rare human centenarian variant of SIRT6 enhances genome stability and interaction with Lamin A

Matthew Simon[1,†] (ID), Jiping Yang[2,†] (ID), Jonathan Gigas[1], Eric J Earley[3] (ID), Eric Hillpot[1], Lei Zhang[4], Maria Zagorulya[1], Greg Tombline[1], Michael Gilbert[5], Samantha L Yuen[4], Alexis Pope[2], Michael Van Meter[1], Stephan Emmrich[1] (ID), Denis Firsanov[1], Advait Athreya[1] (ID), Seyed Ali Biashad[1] (ID), Jeehae Han[6], Seungjin Ryu[6] (ID), Archana Tare[6], Yizhou Zhu[6] (ID), Adam Hudgins[6] (ID), Gil Atzmon[6,7], Nir Barzilai[6], Aaron Wolfe[8] (ID), Kelsey Moody[8], Benjamin A Garcia[5], David D Thomas[4] (ID), Paul D Robbins[4], Jan Vijg[6] (ID), Andrei Seluanov[1,*] (ID), Yousin Suh[2,**] (ID) & Vera Gorbunova[1,***] (ID)

Abstract

Sirtuin 6 (SIRT6) is a deacylase and mono-ADP ribosyl transferase (mADPr) enzyme involved in multiple cellular pathways implicated in aging and metabolism regulation. Targeted sequencing of SIRT6 locus in a population of 450 Ashkenazi Jewish (AJ) centenarians and 550 AJ individuals without a family history of exceptional longevity identified enrichment of a SIRT6 allele containing two linked substitutions (N308K/A313S) in centenarians compared with AJ control individuals. Characterization of this SIRT6 allele (centSIRT6) demonstrated it to be a stronger suppressor of LINE1 retrotransposons, confer enhanced stimulation of DNA double-strand break repair, and more robustly kill cancer cells compared with wild-type SIRT6. Surprisingly, centSIRT6 displayed weaker deacetylase activity, but stronger mADPr activity, over a range of NAD$^+$ concentrations and substrates. Additionally, centSIRT6 displayed a stronger interaction with Lamin A/C (LMNA), which was correlated with enhanced ribosylation of LMNA. Our results suggest that enhanced SIRT6 function contributes to human longevity by improving genome maintenance via increased mADPr activity and enhanced interaction with LMNA.

Introduction

SIRT6 is a protein deacylase and mono-ADP-ribosylase (mADPr) enzyme that has diverse cellular functions, many of which are related to aging and longevity. SIRT6 knockout mice show premature aging and genomic instability (Mostoslavsky et al, 2006) while mice overexpressing SIRT6 display an extended lifespan (Kanfi et al, 2012; Roichman et al, 2021). Across mammalian species, SIRT6 is conserved and its activity has a strong positive correlation with maximum lifespan (Tian et al, 2019). At the molecular level, SIRT6 is involved in DNA repair, telomere maintenance, silencing of the repetitive elements including LINE1 retrotransposons, regulation of glucose homeostasis, inflammation, and pluripotency (Mostoslavsky et al, 2006; Michishita et al, 2008; Kawahara et al, 2009; Mao et al, 2011; Van Meter et al, 2014, 2016; Etchegaray & Mostoslavsky, 2015). In addition, SIRT6 is a noted tumor suppressor (Van Meter et al, 2011; Min et al, 2012; Sebastian et al, 2012). Cells lacking SIRT6 are more susceptible to malignant transformation, while SIRT6 overexpression induces apoptosis in cancer cells but not in normal cells (Van Meter et al, 2011).

1 Department of Biology, University of Rochester, Rochester, NY, USA
2 Department of Obstetrics and Gynecology, Columbia University, New York, NY, USA
3 Biostatistics and Epidemiology, RTI International, Durham, NC, USA
4 Department of Biochemistry, Molecular Biology and Biophysics and Institute on the Biology of Aging and Metabolism, University of Minnesota, Minneapolis, MN, USA
5 Department of Biochemistry and Biophysics, Perelman School of Medicine, University of Pennsylvania, Philadelphia, PA, USA
6 Department of Genetics, Albert Einstein College of Medicine, Bronx, NY, USA
7 Department of Biology, Faculty of Natural Sciences, University of Haifa, Haifa, Israel
8 Ichor Therapeutics, Lafayette, NY, USA
    *Corresponding author. Tel: +1 5852756636; E-mail: andrei.seluanov@rochester.edu
    **Corresponding author. Tel: +1 2123056832; E-mail: ys3214@cumc.columbia.edu
    ***Corresponding author. Tel: +1 5852757740; E-mail: vera.gorbunova@rochester.edu
    †These authors contributed equally to this work

SIRT6 is localized in the nucleus where it interacts with nuclear scaffold protein Lamin A/C (LMNA) (Ghosh *et al*, 2015), which is also implicated in human longevity. Mutations in LMNA cause a multitude of human genetic syndromes, many of them associated with premature aging, including Hutchinson Gilford progeria syndrome (HGPS) (De Sandre-Giovannoli *et al*, 2003; Eriksson *et al*, 2003). Interaction with LMNA activates SIRT6 enzymatic activities (Ghosh *et al*, 2015). Early onset premature aging observed in SIRT6 deficient mice resembles HGPS, which led to the suggestion that abnormal SIRT6 localization and function in HGPS drives the disease pathogenesis (Ghosh *et al*, 2015). A coding change in *SIRT6*, SIRT6 D63H, leads to the loss of SIRT6 enzymatic activity and embryonic lethality (Ferrer *et al*, 2018).

The strong correlation between SIRT6 activity and longevity across species (Tian *et al*, 2019) and in genetically modified mice (Kanfi *et al*, 2012; Roichman *et al*, 2021) raises the question of whether higher SIRT6 activity may be associated with a longer lifespan in humans. Noncoding genetic polymorphisms in the SIRT6 gene region were associated with human longevity in candidate SNP analyses (TenNapel *et al*, 2014; Li *et al*, 2016; Hirvonen *et al*, 2017). To date, no beneficial mutations in *SIRT6* associated with longevity have been functionally characterized.

In this study, we identified two novel variants of *SIRT6* enriched in a population of human centenarians. One of these variants, centSIRT6 possesses altered biological activities compared with the common allele. centSIRT6 allele demonstrates enhanced mono-ADP ribosylase activity but a reduced deacetylase activity *in vitro*. This tradeoff in activity produces an allele that confers enhancement in DNA repair and enhanced suppression of transposable elements, as well as resistance to oxidative stress. Additionally, the centenarian allele is more efficient at killing cancer cells. Functionally, we found that the centenarian allele shows enhanced interaction with LMNA, which correlates with an increased ribosylation state of LMNA. Together, we identified a novel centenarian allele of SIRT6 that results in enhanced genome maintenance by shifting the balance between the deacetylation and mADPr activities of SIRT6.

Results

To examine whether variants of SIRT6 are associated with human longevity we performed targeted sequencing of SIRT6 locus in a population of 450 Ashkenazi Jewish (AJ) centenarians and 550 AJ controls (individuals without a family history of exceptional longevity) (Fig 1A). Table 1 shows all the SNPs identified. We observed an association of rs350845 with living beyond 100 years ($P = 0.009$, Table 1). This SNP lies within a *SIRT6* intron and is an eQTL for *SIRT6* upregulation across 18 tissue types (Fig EV1A–C). Interestingly, this SNP is in high linkage disequilibrium LD ($r^2 > 0.98$) with two other eQTLs, rs350843 and rs350846, which also upregulate *SIRT6*.

In addition, two rare missense variants in perfect linkage were observed, rs183444295 (A313S) and rs201141490 (N308K), aka centSIRT6, which had nearly double the allele frequency among centenarians (1.0%) compared with both study controls (0.55%) and the AJ cohort within GnomAD (0.60%), although this difference was not statistically significant ($P = 0.3$, $P = 0.27$, respectively) due to limited population size.

Analysis of the entire GnomAD database (141,456 individuals of diverse ethnic backgrounds), uncovered an apparent enrichment of centSIRT6 allele pair among the 75+ age group compared with other age groups. Compared with other alleles at similar MAF (0.1–1%), the centSIRT6 allele was in the top 5th percentile of 75+ enriched SNPs and in the 9th percentile of all missense mutations (Fig 1B and C). We sought to characterize this missense mutation to discover its molecular impacts on SIRT6 function in the context of extreme longevity (Fig 1D).

centSIRT6 demonstrates reduced deacetylase activity *in vitro*

SILAC analysis of HEK293 cells expressing different SIRT6 alleles showed no difference in the protein turnover rates between the WT and centSIRT6 (Fig EV2A). To assess the biochemical properties of the different SIRT6 alleles, we generated and purified recombinant protein for each allele (Fig EV2B). Consistent with similar half-lives of wild type and centSIRT6 *in vivo*, we found no notable differences in the thermal stability of the SIRT6 alleles *in vitro*, suggesting that centSIRT6 does not grossly alter the folding or the ambient stability (Fig EV2C).

We then tested SIRT6 deacylase activity (Jiang *et al*, 2013) on a myristoylated peptide to determine K_m for NAD^+ for wild type and centSIRT6. While the centenarian allele displayed a slight reduction in activity (V_{max}) compared with the wild type ($P = 0.02$) (Fig 1E), K_m was not significantly different between wild type and centSIRT6 for both substrates. Quenching of SIRT6 intrinsic Trp fluorescence by NAD^+ binding also showed that centSIRT6 has a similar affinity for NAD^+ to the wild-type allele (Fig EV2D). Overall, these data indicate that centSIRT6 confers a slight reduction in deacylase catalytic efficiency (as defined by V_{max}/K_m) (Fig 1E).

The centSIRT6 displayed significantly lower deacetylase activity and slower kinetics on recombinant nucleosomes with saturated H3K9ac and H3K18ac modifications (Fig 2A and B). Similar to the synthetic histones, the centSIRT6 allele deacetylated both H3K9ac and H3K18ac residues on nucleosomes purified from HeLa cells, at a significantly reduced activity compared with the wild-type SIRT6 (Fig EV3A). Taken together, the combined data from deacylase and histone deacetylase experiments indicate that the centSIRT6 variant has reduced deacylase/deacetylase activity.

To test the effect of the centSIRT6 allele on histone deacetylation activity *in vivo*, we generated telomerase-immortalized human HCA2 fibroblast cell lines in a SIRT6 KO background containing a cumate switch promoter driving expression of SIRT6 WT, N308K, A313S, and the centSIRT6 alleles (cumate SIRT6 fibroblasts). Each cell line was induced with cumate to drive equal and robust levels of SIRT6 expression (Fig EV3B and C). To rule out contributions from cumate to cell viability and toxicity, cells were assessed for apoptosis and growth rate and no differences were noted (Fig EV3D and E). We quantified histone post-translational modifications from purified histones (Fig EV3F) from these cells by mass spectrometry using peptide standards as described previously (Sidoli *et al*, 2016). Cells expressing the centSIRT6, N308K, and A313S SIRT6 alleles showed similar global histone post-translational modification (PTM) levels at all sites known to be SIRT6 substrates including H3K9ac, H3K18ac, and H3K56ac (Fig 2C; Dataset EV1). Similarly, global levels of H3K9ac and H3K18ac measured by Western blot did not show significant changes, even when challenged with paraquat-

A

Group	Female	Male	Age (mean±SD)	BMI (mean±SD)
Control	289	261	78.3 ± 8.1	26.9±4.8
Cent	333	117	100.4 ± 3.3	22.8±3.6

B

C

D

CGGATCAACGGCTCTATCCCCGCCGGCCCC **WT**

CGGATCAAGGGCTCTATCCCCTCCGGCCCC **Centenarian**

Asp to Lys (N308K)   Ala to Ser (A313S)

E

	Km$_{NAD}$ (µM)	Km$_{pep}$ (µM)	Vmax (RFU/s)	Vmax/Km$_{pep}$
WT	55.5 ± 5.4	61.1 ± 12.4	37.2 ± 4.1	0.61
Cent	48.4 ± 3.7	46 ± 11.3	24.3 ± 2.9*	0.53
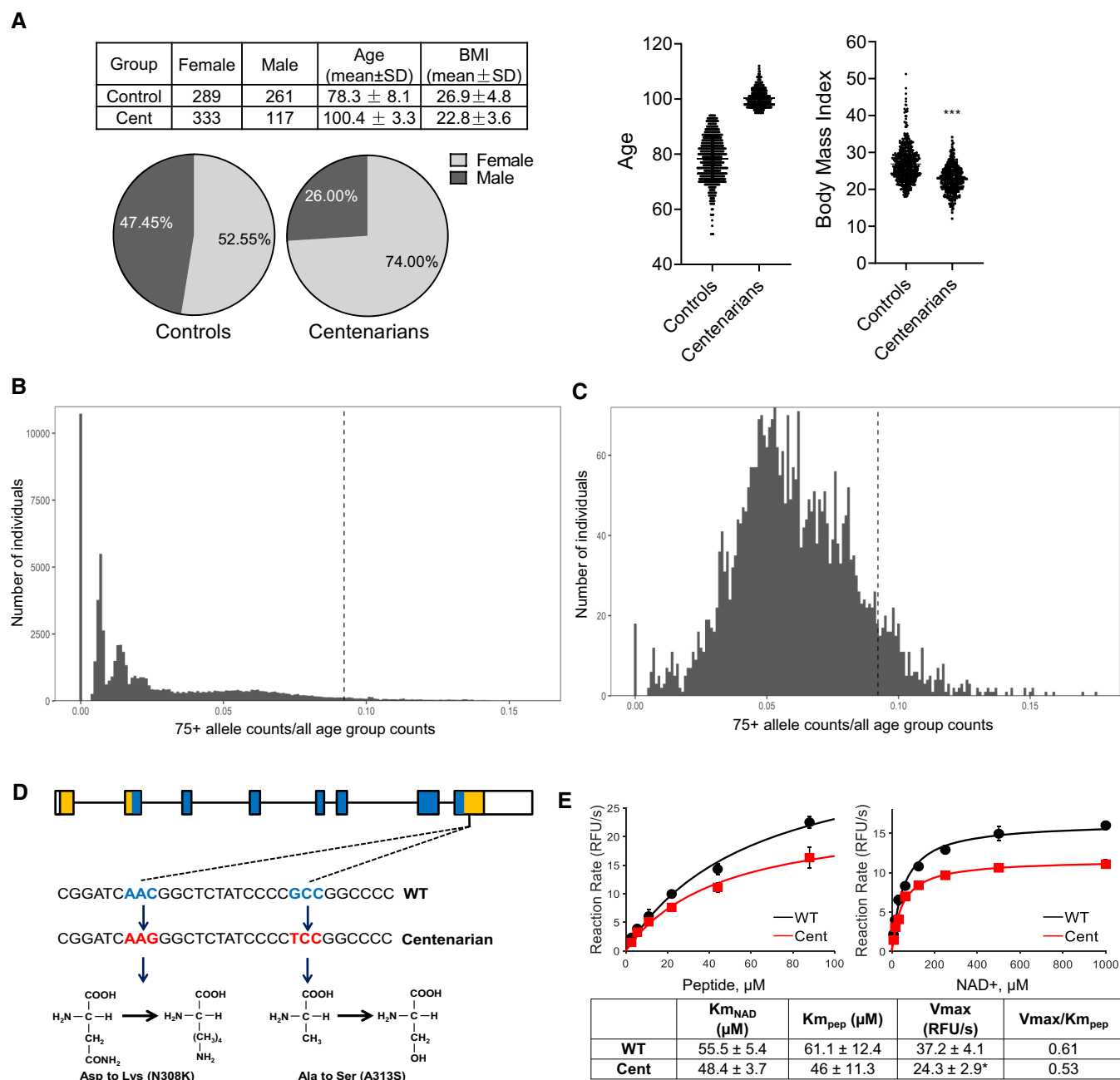
Figure 1. CentSIRT6 missense variant identified in AJ centenarians demonstrates lower deacetylation activity.

A   Age, gender, and BMI information of the Ashkenazi Jewish Centenarian cohort. Table showing the age, gender, and BMI information in control and centenarian groups. Pie chart showing the percentage of male/female individuals in control and centenarian groups. Right panel showing the age and BMI distribution of all individuals recruited in targeted capture-seq. Data were presented as mean and SD. Student's *t*-test, two-tailed, ***$P < 0.001$.

B, C Histograms of normalized allele counts in individuals 75+ years old compared with all age groups ($N = 125,748$) across (B) all chromosome 19 SNPs and small insertions/deletions, and (C) missense SNPs and indels only. Dotted vertical lines show centSIRT6.

D   The structure of the SIRT6 gene. centSIRT6 contains two missense mutations in the C-terminus N308K and A313S. White boxes represent UTRs, colored boxes represent protein-coding regions, and blue boxes represent enzymatic domains.

E   Michaelis–Menten kinetic parameters as calculated by saturation curves using the differential concentrations of myristoylated peptide or NAD$^+$. $n = 3$ technical replicates (TR); error bars = SD.

induced oxidative damage (Fig 2D). We then sought to evaluate more direct targets of SIRT6's deacetylase activity by performing ChIP using antibodies to H3K9ac and H3K18ac. Previous reports have identified LMNA, MsSOD, NFκB2, and NFκBia as H3K9ac targets of SIRT6, as well as SatII and SatIII as H3K18ac targets (Kawahara *et al*, 2009, 2011; Tasselli *et al*, 2016). However, similar to

Table 1. List of all SIRT6 variants identified by capture sequencing.

SNP ID	Alt	Ref	Variant Type	AA change	Current study centenarians			Current study controls				GnomAD controls			
					Alt Count	Ref Count	MAF	Alt Count	Ref Count	MAF	P	Alt Count	Ref Count	MAF	P
rs350845	G	A	Intron	–	749	151	0.17	962	138	0.126	0.009	8,783	1,367	0.135	0.007
rs11554579	C	T	Synonym	R76R	13	887	0.014	10	1,090	0.009	0.296	91	9,785	0.009	0.15
rs183444295	**A**	**C**	**Missense**	**A313S**	**9**	**891**	**0.010**	**6**	**1,094**	**0.006**	**0.3**	**25**	**4,281**	**0.006**	**0.267**
rs201141490	**C**	**G**	**Missense**	**N308K**								**28**	**4,826**	**0.006**	**0.268**
rs748302927	T	G	Intron	–	1	899	0	0	1,100	0	0.45	5	9,375	5E-04	0.423
rs992892719	G	C	Missense	R291P	24	876	0.03	27	1,073	0.025	0.777	0	6,726	0	<0.001
rs200174862	T	G	Intron	–	1	899	0	1	1,099	9E-04	1	3	4,777	6E-04	0.499
rs200813796	T	C	3'UTR	–	3	897	0	3	1,097	0.003	1	11	4,075	0.003	0.728

AJ, Ashkenazi Jewish; MAF, minor allele frequency; REF, reference allele; ALT, alternative allele; CON, controls; CENT, centenarians; P-values from the Fisher exact test on allele counts. Bold values correspond to the SNPs present in the Centenarian Variant of SIRT6 used in the other experiments.

what was observed for global histone acetylation, no major differences were observed between the WT and centSIRT6 alleles, though both alleles were capable of reduced acetylation at these target sites compared with the uninduced cells (Fig 2E–J). These results suggest that while centSIRT6 enzyme has reduced catalytic efficiency of deacetylation, its activity is sufficient to maintain normal steady-state levels of PTMs *in vivo*.

mADPr activity is enhanced in centSIRT6

In addition to its deacetylase activity, SIRT6 has mono-ADP ribosylation (mADPr) activity, able to mono-ADP ribosylate itself and other proteins. mADPr activity is critical to SIRT6 role in DNA damage response and LINE1 repression (Kaidi *et al*, 2010; Mao *et al*, 2011; Van Meter *et al*, 2014). To assess the mADPr activity, two known SIRT6 substrates were used: PARP1 and SIRT6, itself. The centSIRT6 demonstrated an enhanced auto-ribosylation rate with biotin-labeled NAD$^+$ than the wild-type SIRT6 protein (Fig 3A). The SIRT6 proteins with single SNPs did not display a notable difference

in self-mADPr compared with the wild type, suggesting the increase observed in the centenarian allele results from a synthetic interaction that is not cumulative between the two SNPs (Fig 3A). Following this, we utilized an antibody (Bonfiglio *et al*, 2020) with specificity to mADPr residues to examine the self-ribosylation efficiency using a titration of NAD$^+$. As with the biotin-labeled NAD$^+$, centSIRT6 displayed almost 2-fold higher maximal mADPr activity and the trend of enhanced activity was also observed upon titration of NAD$^+$ (Fig 3B). After subtraction of the basal signal where zero NAD$^+$ was added, Michaelis–Menten best-fit analysis of the horse-radish peroxidase signals revealed that CentSIRT6 displayed an apparent NAD$^+$ affinity (K_{app} NAD) of 223 µM and maximal relative auto-ribosylation signal mADPr$_{max}$ of 5.2e^6, whereas wild-type SIRT6 displayed K_{app} NAD =54.2 µM and mADPr$_{max}$ of 1.85e^6 (Fig 3B). In *trans*, mADPr activity was assessed by incubation with human PARP1, which was previously shown to be ribosylated by SIRT6 (Mao *et al*, 2011). Similar to self-ribosylation, the centSIRT6 protein displayed higher PARP1 ribosylation activity (Fig 3C). While both single mutants had elevated activity, the A313S protein was

---

Figure 2. CentSIRT6 possesses reduced deacetylase activity.

A, B Deacetylase activity on H3K9 (A) and H3K18 (B) residues shows reduced activity in centSIRT6 allele. Designer histones were incubated with purified SIRT6 and 5 mM NAD$^+$, then resolved by SDS–PAGE and analyzed by immunoblotting with acetyl-specific histone antibodies. n = 3 TR; error bars = SD. Student's *t*-test, two-tailed. Asterisks indicate P < 0.05 compared with WT, color corresponds to allele. H3K9ac, H3K18ac, and H3 are blots, SIRT6 loading Coomassie stain HeLa histone preps were also probed as shown in Fig EV3A.

C Quantitative mass spec of histone H3 peptide purified from human cells expressing different SIRT6 alleles did not reveal a difference in acetylation levels. Relative fraction represents the portion of the peptide encompassing H3K9–17 compared with the summed total of all of the peptide quantitation values for the same region. Acetylation of other H3 peptides is shown in Supplementary Data 1. Histone preparation is shown in Fig EV3F. n = 3 biological replicates (BR); error bars = SD. Student's *t*-test, two-tailed.

D Whole cell histone H3 acetylation levels in cumate-inducible SIRT6 human fibroblasts, assessed by Western blot. Cu, cumate; PQ, paraquat. Cumate dosage required for equivalent SIRT6 protein abundance was determined by Western blot and administered accordingly to respective cell lines (Fig EV3B and C). Cells were incubated with an appropriate cumate dose for 48 h prior to harvest, with PQ-treated cells receiving PQ 24 h after initial cumate induction.

E–H Relative abundance of H3K9ac at SIRT6-dependent NF-κB target genes. Anti-H3K9ac antibodies were used to perform ChIP in the absence (−Cu) or presence of (+Cu) cumate-induced SIRT6 expression. Samples were normalized using 10% input. n = 3 BR; error bars = SD. Student's *t*-test, two-tailed. Black asterisks indicate P < 0.05 compared with −Cu condition. Red asterisks indicate P < 0.05 compared with +Cu WT.

I, J Relative abundance of H3K18ac at satellite repeats associated with SIRT6 deacetylase activity. Anti-H3K18ac antibodies were used to perform ChIP in the absence (−Cu) or presence of (+Cu) cumate-induced SIRT6 expression. Samples were normalized using 10% input. n = 3 TR; error bars = SD. Student's *t*-test, two-tailed. Black asterisks indicate P < 0.05 compared with −Cu condition.

Source data are available online for this figure.
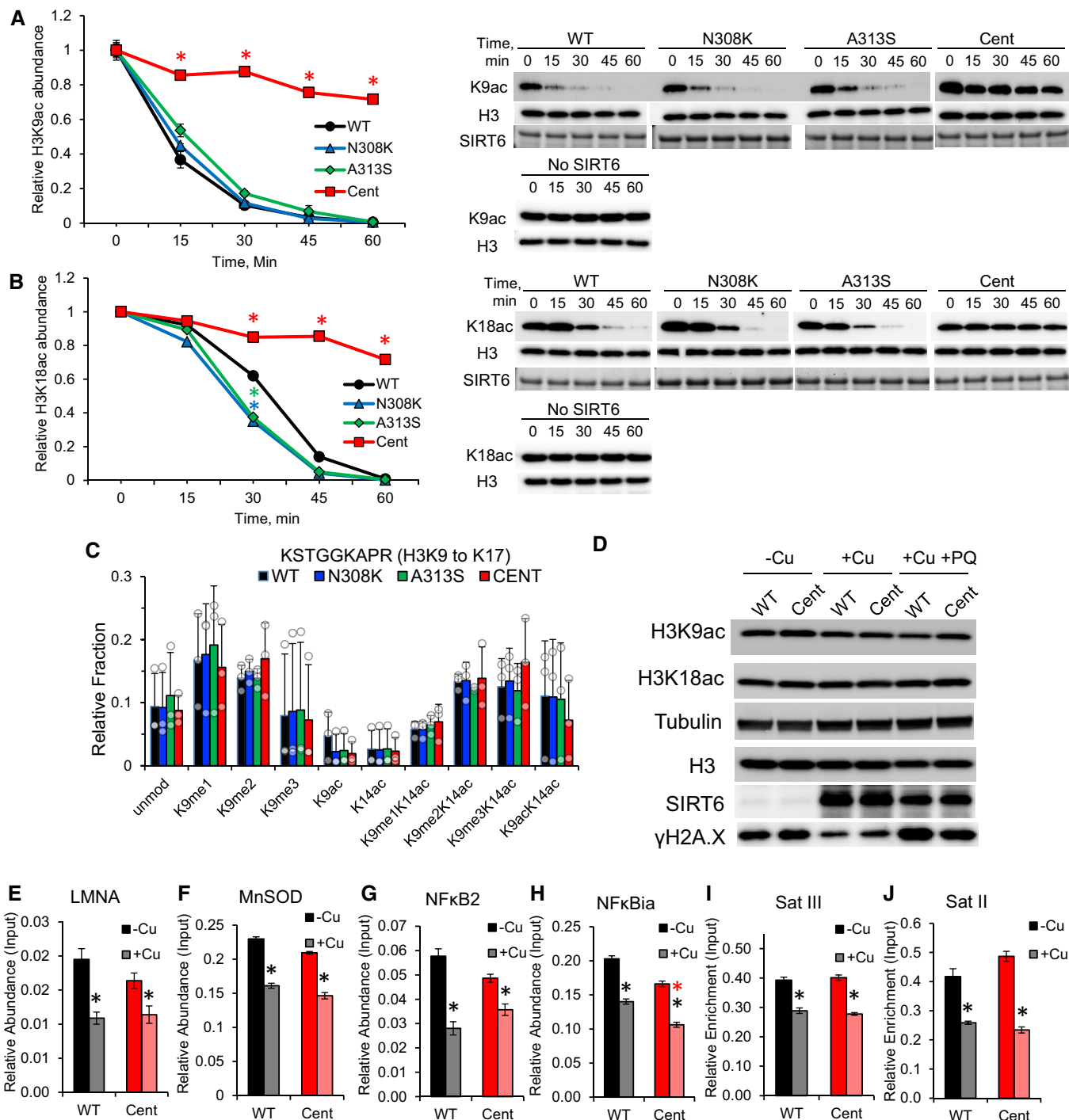
Figure 2.

more similar to the centSIRT6 than N308K (Fig 3C). Collectively, these data show that centSIRT6 displays enhanced mADPr activity.

centSIRT6 is more efficient at suppressing LINE1s and cancer cell killing

SIRT6 suppresses the expression of LINE1 retrotransposons via its mADPr activity (Van Meter *et al*, 2014). The loss of silencing of these elements contributes to age-related sterile inflammation and drives progeroid phenotypes in SIRT6 KO mice (Simon *et al*, 2019). To assess the capacity of the centSIRT6 allele to silence LINE1 transposons, we used the cumate-inducible fibroblasts expressing alleles of SIRT6. qRT–PCR analysis of both 5′- and 3′-biased regions of an evolutionarily active family of human LINE1s (L1HS) both showed that the centSIRT6 allele enhances LINE1 suppression compared with the wild-type SIRT6, as did the N308K allele (Fig 4A). The

Figure 3. CentSIRT6 demonstrates enhanced mADPr activity.

A   Self-ribosylation of SIRT6 using biotin-labeled NAD$^+$. Recombinant SIRT6 was incubated with NAD$^+$ conjugated with a biotin residue and then run on an SDS–PAGE. Each allele was assessed relative to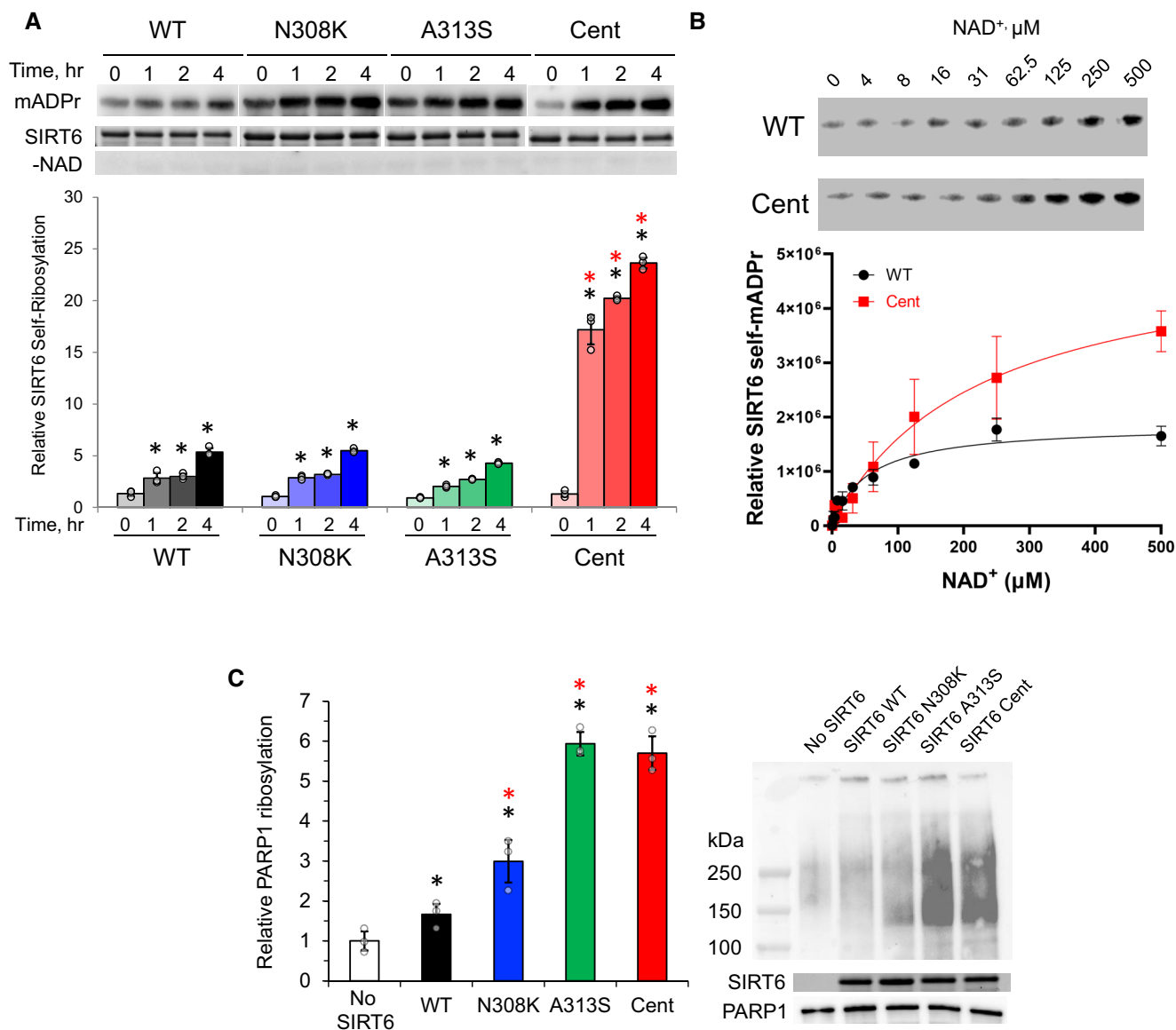 its 0 h time point and normalized to SIRT6 total protein loading controls. $n = 3$ TR; error bars = SD. Student's t-test, two-tailed. Asterisks indicate $P < 0.05$. Black asterisks indicate significance over 0 h control. Red asterisks indicate significance over time-matched WT SIRT6.

B   Self-ribosylation of SIRT6 with titration of NAD$^+$. mADPr-specific antibody (Bonfiglio *et al*, 2020) was used to detect ribosylated wild-type SIRT6 and centSIRT6 proteins. Plot fits the Michaelis–Menten best-fit with GraphPad software. $K_{m\ NAD}$ was 142 ± 29 for centSIRT6 and 106 ± 45 for wild-type SIRT6, and the maximal signal was ~2x greater for centSIRT6 compared with the wild-type SIRT6. Two separate batches of recombinant protein of each SIRT6 allele were prepared and assayed. $n = 3$ TR; error bars = SD.

C   Activation of PARP1 by SIRT6 variants. SIRT6 protein was incubated with human PARP1 protein and then analyzed by immunoblotting with poly-ADPr antibody. Poly-ADPr activity of PARP1 results in a wide range of product size. Activity was assessed by quantifying poly-ADPr signal in whole lanes for each sample. $n = 3$ TR; error bars = SD. Two-way ANOVA. Asterisks indicate $P < 0.05$. Black asterisks indicate significance over HPRT control. Red asterisks indicate significance over wild-type SIRT6.

Source data are available online for this figure.

A313S allele showed a slight trend toward stronger suppression but did not show a significant improvement over the wild-type SIRT6 when assessed for the 3′ bias. We then examined whether the centSIRT6 allele could directly inhibit LINE1 retrotransposition

(RT). HCA2 cells expressing centSIRT6 demonstrated a significant reduction in successful RT events compared with wild-type SIRT6 (Fig 4B). Previous reports have demonstrated that SIRT6 executes LINE1 silencing via ribosylation of the heterochromatin scaffold

protein, KAP1 (Van Meter *et al*, 2014). centSIRT6 was more efficient than the wild-type SIRT6 at ribosylating KAP1 *in vitro* (Fig 4C). These results show that centSIRT6 is more efficient at silencing LINE1 elements, possibly through enhanced ribosylation of KAP1, which are functionally implicated in longevity.

SIRT6 is a major regulator of DNA double-strand break (DSB) repair (Mao *et al*, 2011). To quantify the differences between the SIRT6 alleles in promoting DSB repair, we employed *in vivo* GFP-based assays that measure nonhomologous end joining (NHEJ) and homologous recombination (HR) repair of a chromosomal DSB induced by I-SceI enzyme (Seluanov *et al*, 2010). Different alleles of SIRT6 were transiently expressed in the NHEJ and HR reporter telomerase-immortalized human foreskin fibroblast cell lines (Mao *et al*, 2008). We found that equivalent amounts of the centSIRT6 stimulated NHEJ 2.5-fold and HR 2-fold greater than the wild-type SIRT6 (Figs 4D and E, and EV4A). Similarly, we observed in the
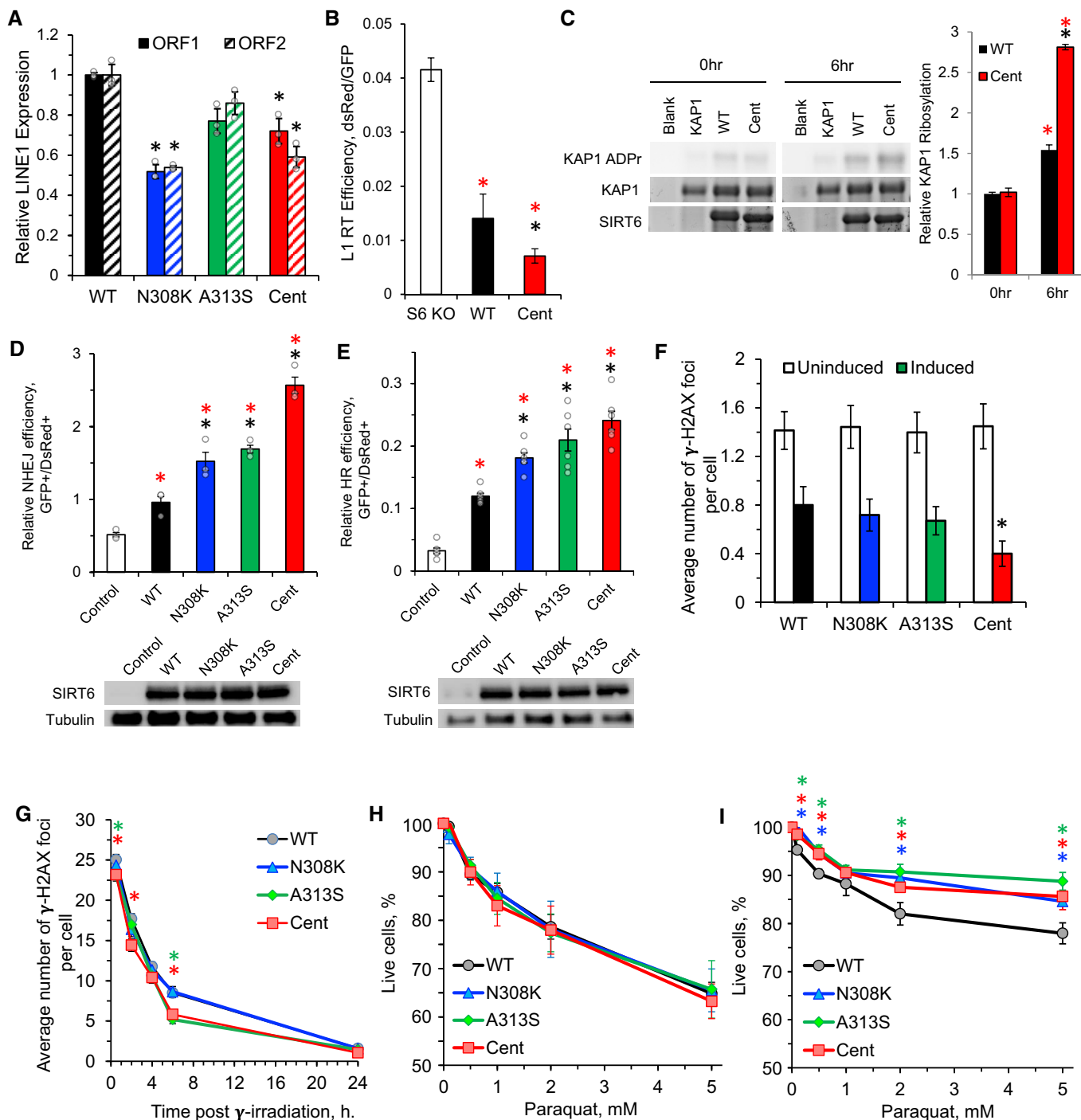

Figure 4.

Figure 4. CentSIRT6 enhances LINE1 retrotransposon suppression and DNA repair.

A   qRT–PCR analysis of LINE1 expression in cumate-inducible SIRT6 fibroblasts. Primers assessed both 5′ (ORF1) and 3′ (ORF2) LINE1 sequences from the L1HS family of evolutionarily active LINE1 retrotransposons. Assessment of both regions was conducted to mitigate contributions from partial insertion sequences in coding genes. Asterisks indicate $P < 0.05$. $n = 3$ TR; error bars = SD. Student's t-test, two-tailed.

B   LINE1 EGFP retrotransposition assay. Three independent transfections with LINE1 EGFP reporter plasmid were conducted and quantified by flow cytometry. Asterisks indicate $P < 0.05$. Red asterisks indicate significance over SIRT6 KO control. Black asterisks indicate significance over WT SIRT6. $n = 3$ BR; error bars = SD. Two-way ANOVA.

C   In vitro KAP1 ribosylation by SIRT6. Asterisks indicate $P < 0.05$. Red asterisks indicate significance over 0 h, black asterisks indicate significance over compared with WT SIRT6. $n = 3$ BR; error bars = SD. Student's t-test, two-tailed.

D, E   Stimulation of NHEJ and HR by SIRT6 variants. Reporter cell lines were co-transfected with SIRT6-expressing plasmid, I-Sce1 plasmid, and DsRed transfection control. After 72 h recovery, reactivation of the GFP reporter was measured by flow cytometry. Stimulation of NHEJ or HR was calculated as the ratio of GFP⁺/DsRed⁺ positive cells. Representative FACS traces are shown in Fig EV4A. Blots demonstrate equivalent SIRT6 abundance in transfected cells. Asterisks indicate $P < 0.05$. Black asterisks indicate significance over control; red asterisks indicate significance over WT SIRT6. $n = 3$ BR; error bars = SD. Two-way ANOVA.

F   Basal γH2AX foci in cumate-inducible SIRT6 fibroblasts. Foci were scored in at least 80 cells per condition. Representative images of the foci are shown in Fig EV4B. Asterisks indicate $P < 0.05$. $n = 3$ BR; error bars = SD. Student's t-test, two-tailed.

G   DNA repair kinetics in cumate-inducible SIRT6 fibroblasts. Cells were grown on slides and irradiated with 2 Gy gamma radiation, followed by immunostaining for γH2AX. Irradiation was conducted when the cells were at 75% confluency on slides. Cells were fixed and foci scored at $t = 0.5$ h, 2 h, 4 h, 6 h, and 24 h postirradiation. Foci were scored in at least 80 cells per genotype per time point. Representative images of the foci are shown in Fig EV4C. Asterisks indicate $P < 0.05$. Asterisks indicate significance over WT SIRT6. Color of the asterisk corresponds to the SIRT6 allele. $n = 3$ BR; error bars = SD. Student's t-test, two-tailed.

H, I   Oxidative stress resistance. Cumate-inducible SIRT6 fibroblasts were induced for SIRT6 expression and exposed to paraquat for 24 h. Resistance was determined by apoptosis staining 48 h after exposure. Representative FACS traces are shown Fig EV4D. Asterisks indicate $P < 0.05$. Asterisks indicate significance over WT SIRT6. Color of the asterisk corresponds to the SIRT6 allele. $n = 3$ BR; error bars = SD. Student's t-test, two-tailed.

Source data are available online for this figure.

cumate SIRT6 fibroblasts expressing centSIRT6 that basal levels of γH2AX foci were reduced by 50% relative to those observed in either single alleles or the wild-type SIRT6 (Figs 4F and EV4B). Taken together, these data indicate that the centSIRT6 allele elicits enhanced DNA DSB repair activity. We next compared whether different SIRT6 alleles have different effects on stress. Using the cumate SIRT6 fibroblasts, we exposed the cells to γ-radiation and assessed the resolution of DSBs over time via γH2AX immunostaining. We observed that while both wild-type and centSIRT6-expressing cell lines had similar levels of γH2AX foci immediately after exposure, the centSIRT6-expressing cells showed an improved recovery rate (Figs 4G and EV4C). In the absence of cumate induction, all cell lines showed no significant differences in survival after oxidative stress (Fig 4H). By contrast, we found that the centSIRT6-expressing cells more resistant to oxidative stress-induced apoptosis (Figs 4I and EV4D). Taken together, these results indicate that the centSIRT6 improves DSB repair and resistance to DNA damage.

To further confirm that centSIRT6 enhances genome maintenance we generated knock-in human embryonic stem cells carrying centSIRT6 allele. The two centenarian mutations were introduced using CRISPR/Cas9 and confirmed by sequencing. We generated two independent knock-in clones and differentiated them into mesenchymal stem cells (MSCs). The MSCs were then transfected with linearized NHEJ and HR GFP reporters (Mao et al, 2008). Cells harboring centSIRT6 allele showed higher efficiency of repair (Fig EV5A and B). These cells were also showed increased survival and a lower number of 53BP1 foci upon treatment with methyl methanesulfonate (MMS), a potent DNA-damaging agent (Fig EV5C and D).

Previous studies have demonstrated that MSCs deficient for SIRT6 have repression of the NRF2-antioxidant mediated stress response (Pan et al, 2016; Rezazadeh et al, 2019). Both RNAseq analysis and qRT–PCR of these target genes, as well as NRF2, showed no significant change between the two alleles (Fig EV5E and F). Interestingly, the centSIRT6 knock-in cells showed higher protein levels of SIRT6 (Fig EV5G), suggesting that centenarian mutations increase protein abundance, in addition to modulating SIRT6 enzymatic activities. As it was impossible to compare equal levels of SIRT6 in CRISPR knock-in cells, we relied on cumate cells for the majority of our in vivo assays.

SIRT6 overexpression induces apoptosis in cancer cells but not in normal cells (Van Meter et al, 2011). In order to assess the tumor cell killing capacity of the centSIRT6 allele, we transfected SIRT6 alleles into two common tumor cell lines, HT1080 and HeLa cells. Expression of the centSIRT6 resulted in ~2-fold fewer adherent surviving cells in both cancer cell lines compared with wild-type SIRT6 (Fig 5A). Additionally, the centSIRT6 allele triggered at least 2-fold higher levels of apoptosis than the wild-type SIRT6 allele in these cancer cell lines (Fig 5B and C). These data indicate that centSIRT6 confers a more robust anti-tumor activity than the wild-type SIRT6.

centSIRT6 displays a higher affinity for LMNA

Since the centSIRT6 mutations are located in the flexible C-terminus of SIRT6 and may influence protein–protein interactions, we compared the interactomes of the centSIRT6 and the wild-type alleles.

Figure 5. CentSIRT6 induces increased cell death in cancer cells.

A   Number of adherent cells after transfection with SIRT6 variants. Cells were transfected with SIRT6 plasmids encoding different SIRT6 alleles and cell numbers were counted after 72 h. HCA2 are normal human foreskin fibroblasts. Asterisks indicate $P < 0.05$. $n = 3$ BR; error bars = SD. Student's t-test, two-tailed.

B, C   Apoptosis staining of cancer cell lines 48 h after transfection. Cells were stained with Annexin V/PI and analyzed by flow cytometry. Asterisks indicate $P < 0.05$. Red asterisks indicate significance over control, black asterisks indicate significance over WT SIRT6.
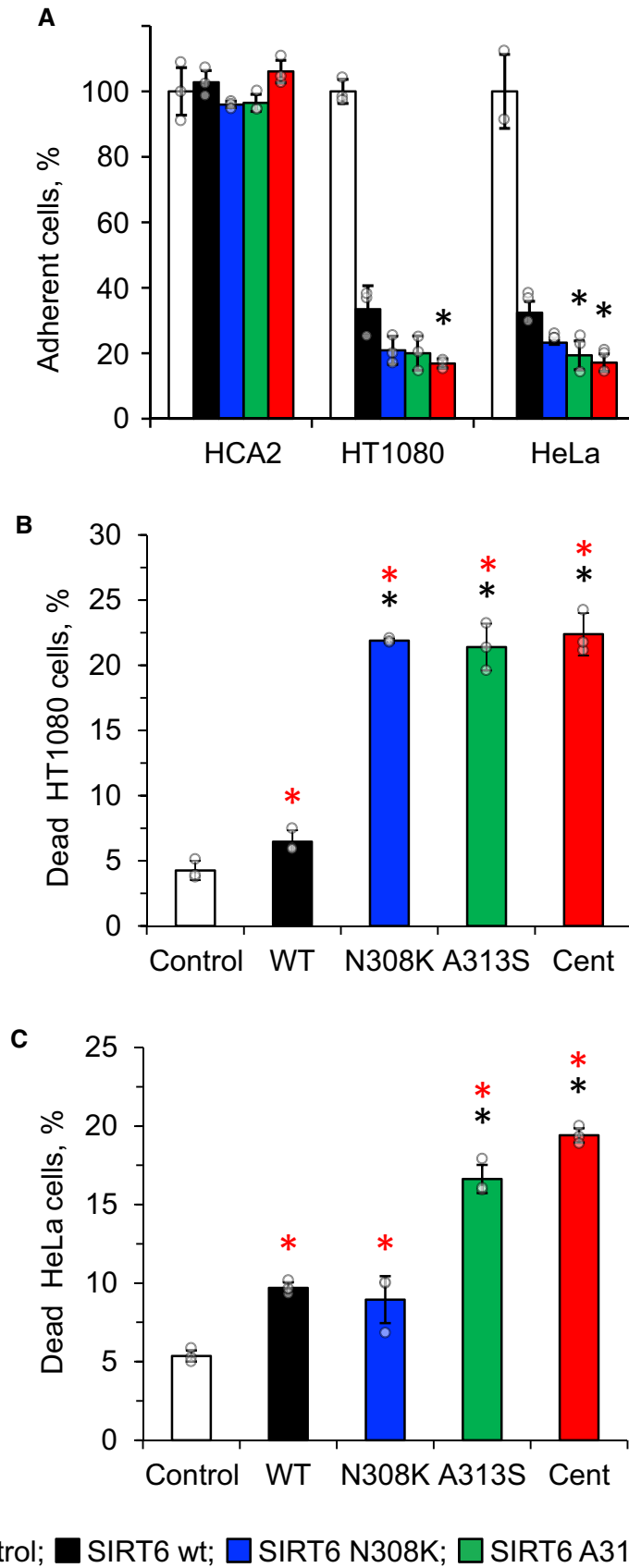
$n = 3$ BR; error bars = SD. Two-way ANOVA.

A

B

C

☐ Control; ■ SIRT6 wt; ■ SIRT6 N308K; ■ SIRT6 A313S; ■ CentSIRT6

Figure 5.

We used antibodies against SIRT6 to immuno-precipitate SIRT6-interacting proteins from cumate SIRT6 fibroblasts and analyzed them by mass spectrometry with tandem mass tags (TMT) to permit accurate quantitation. Several interacting proteins were enriched by the centSIRT6 allele (Fig 6A; Dataset EV2). Most notable proteins showing stronger interaction with centSIRT6 than the wild-type

SIRT6 were LMNA and vimentin (VIME), which showed 38 and 40 peptides, respectively. Both of these proteins are known to interact with SIRT6 (Patil & Nakamura, 2005; Ghosh et al, 2015; Huttlin et al, 2015; Gioutlakis et al, 2017; Oughtred et al, 2019), and LMNA was shown to stimulate SIRT6 activity (Ghosh et al, 2015). No loss or gain of interactions was apparent in the centSIRT6 set, indicating

A

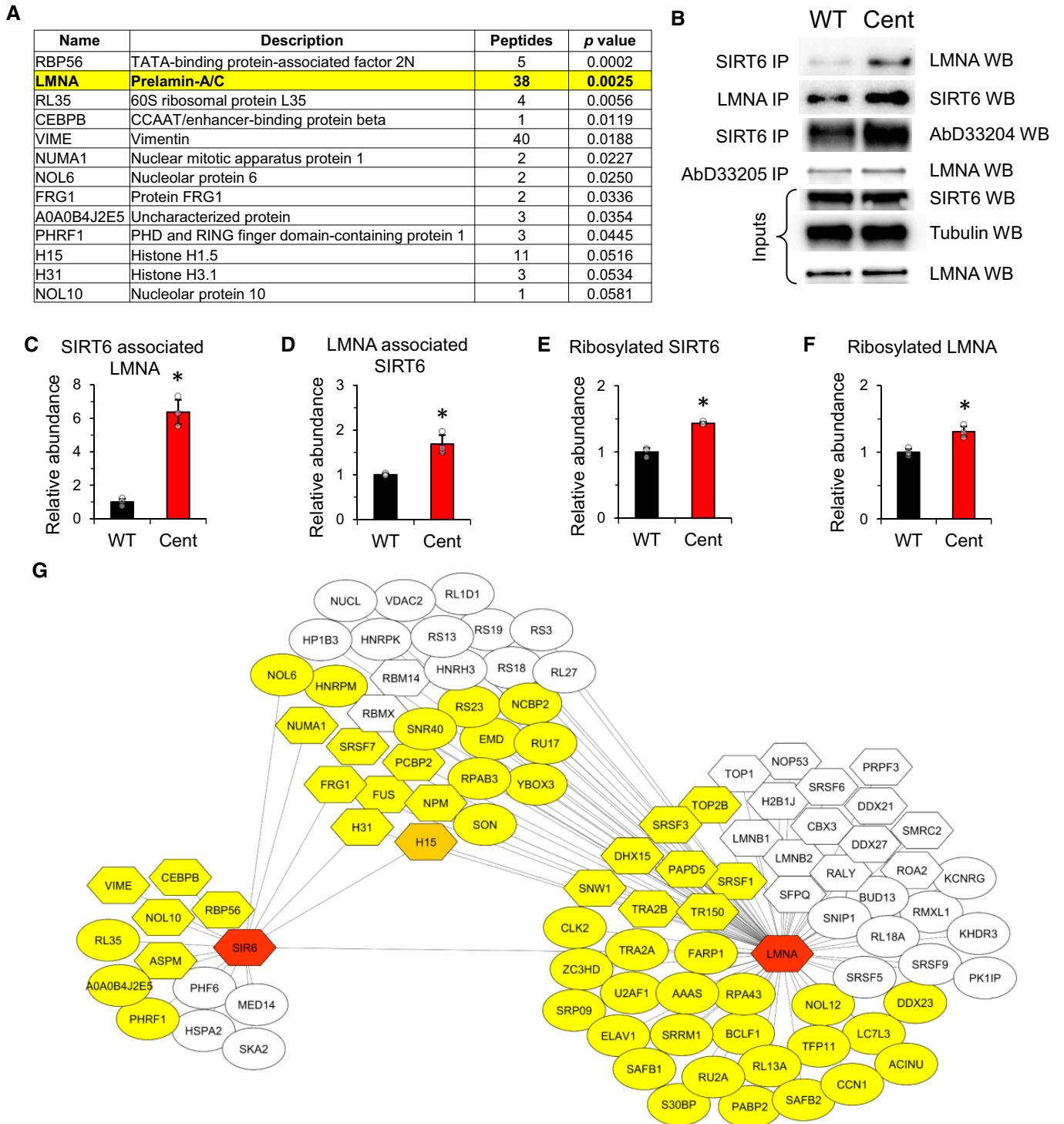| Name	Description	Peptides	*p* value
RBP56	TATA-binding protein-associated factor 2N	5	0.0002
LMNA	**Prelamin-A/C**	**38**	**0.0025**
RL35	60S ribosomal protein L35	4	0.0056
CEBPB	CCAAT/enhancer-binding protein beta	1	0.0119
VIME	Vimentin	40	0.0188
NUMA1	Nuclear mitotic apparatus protein 1	2	0.0227
NOL6	Nucleolar protein 6	2	0.0250
FRG1	Protein FRG1	2	0.0336
A0A0B4J2E5	Uncharacterized protein	3	0.0354
PHRF1	PHD and RING finger domain-containing protein 1	3	0.0445
H15	Histone H1.5	11	0.0516
H31	Histone H3.1	3	0.0534
NOL10	Nucleolar protein 10	1	0.0581

Figure 6.

Figure 6. CentSIRT6 allele shows enhanced interaction with LMNA.

A   Proteins showing stronger interaction with centSIRT6 compared with the wild-type SIRT6. Proteins were prepared from cumate-induced SIRT6 cell lines and immuno-precipitated with SIRT6 antibody; rabbit preimmune serum was used as a control. Prior to analysis by mass spectrometry, samples were labeled with tandem mass tags.
B   IP experiments on lysates from cumate-induced fibroblasts expressing wild-type or centSIRT6 alleles with antibodies to SIRT6, LMNA, and mADPr. SIRT6 expression was induced 48 h prior to IP. n = 3 BR. One representative set of IPs is shown.
C   CentSIRT6 shows stronger interaction with LMNA compared with the wild-type SIRT6. Quantification of the IP experiment shown in (B). SIRT6 IP followed by Western blot with antibodies to LMNA.
D   LMNA shows enhanced interaction with centSIRT6 compared with wild type. Quantification of the IP experiment shown in (B). LMNA IP from cumate-inducible SIRT6 fibroblasts followed by Western blot with antibodies to SIRT6.
E   centSIRT6 shows enhanced mADPr. Quantification of the IP experiment shown in (B). SIRT6 IP from cumate-inducible SIRT6 fibroblasts followed by Western blot with antibody to mADPr residues (Bonfiglio *et al*, 2020).
F   LMNA shows an enhanced mADPr signal in cells expressing centSIRT6. Quantification of the IP experiment shown in (B). IP with mADPr antibody (Bonfiglio *et al*, 2020) using extract from cumate-induced SIRT6 fibroblasts, followed by Western blot with antibodies to LMNA.
G   SIRT6 and LMNA are colored red and featured as central points in two opposing nodes of interactions. A third node (upper middle) shows interaction partners that are shared by SIRT6 and LMNA. Proteins whose interactions are enhanced by the centSIRT6 allele are colored yellow. Proteins that interacted equally with wild-type and centSIRT6 alleles are uncolored. H1.5 is a special case and colored orange because it showed increased interaction with the centSIRT6 and decreased interaction with LMNA in the presence of the centSIRT6 allele. Proteins known to be ribosylated in previous reports are shown as hexagons.

Data information: For C–F, n = 3 BR; error bars = SD. Student's *t*-test, two-tailed. Asterisks indicate *P* < 0.05.

Source data are available online for this figure.

that the effect of the novel allele could be in enhancing existing SIRT6 interactions.

LMNA is a nuclear scaffold protein playing a central role in nuclear organization and is also implicated in aging. To confirm the mass spec data on SIRT6 and LMNA interactions, we performed co-IP with SIRT6 antibodies followed by Western blot with LMNA antibodies using cumate SIRT6 fibroblasts. We found that centSIRT6, indeed, associates more strongly with LMNA than the wild-type SIRT6 allele (Fig 6B and C), and the effect was reciprocal as assessed by co-IP with LMNA antibodies followed by Western blot with SIRT6 antibodies (Fig 6B and D). Taken together these results demonstrate that centSIRT6 interacts more strongly with LMNA than the wild-type SIRT6. Given the enhanced mADPr activity of the centSIRT6 allele, we next assessed the ribosylation status of LMNA using the mADPr antibodies. SIRT6 IPs performed on the cumate SIRT6 fibroblasts, using the mADPr-specific antibody (Bonfiglio *et al*, 2020), showed that centSIRT6 was more ribosylated *in vivo* (Fig 6B and E); as demonstrated *in vitro* with the purified SIRT6 proteins (Fig 3A). We also conducted IPs against vimentin and TAF15 (RBP56), as both also demonstrated enhanced association with centSIRT6. Additionally, TAF15 has also been shown to be ribosylated in response to genotoxic stress (Jungmichel *et al*, 2013). The IPs revealed enhanced ribosylation status of vimentin and TAF15 in centSIRT6-expressing cells (Appendix Fig S2A–C). IP with a mADPr-specific antibody (Bonfiglio *et al*, 2020) and subsequent Western blot with an anti-LMNA antibody revealed increased ribosylation of LMNA in the presence of the centSIRT6 allele (Fig 6B and F). LMNA has been reported to be ADP-ribosylated *in vivo* on several residues (Adolph & Song, 1985; Adolph, 1987; Hendriks *et al*, 2019).

We hypothesized that the centSIRT6 allele may influence the interaction of LMNA with other proteins. To test this, we immunoprecipitated LMNA from the cumate fibroblasts expressing either the wild-type SIRT6 or centSIRT6 alleles and performed quantitative protein interaction analysis using TMT labeling followed by mass spectrometry. While many proteins showed similar interaction with LMNA, regardless of the SIRT6 allele present, a large group of proteins showed enhanced interaction with LMNA in the presence of

centSIRT6 (Fig 6G; Dataset EV3). LMNA-interaction partners enhanced by centSIRT6 included ELAVL1, FUS, PCBP2, SAFB, SRSF1, SRSF3, TFIP11, THRAP3, BCLAF1, and U2AFBP. All proteins facilitate the coordination of the DNA damage response with RNA processing (Beli *et al*, 2012; Montecucco & Biamonti, 2013; Naro *et al*, 2015; Vohhodina *et al*, 2017). Many of the proteins identified in SIRT6 and LMNA IPs are ADP-ribosylated (Jungmichel *et al*, 2013; Martello *et al*, 2016; Bilan *et al*, 2017; Vivelo *et al*, 2017; Leslie Pedrioli *et al*, 2018; Hendriks *et al*, 2019) (shown as hexagons in Fig 6G), suggesting that ADP ribosylation by SIRT6 may play a role in mediating these interactions. Taken together, our data show that centSIRT6 is more efficient at promoting DNA repair and suppressing LINE1 elements, which is likely mediated by its enhanced mADPr activity and stronger interaction with LMNA.

Discussion

We demonstrated that a novel rare variant of SIRT6 discovered in a cohort of centenarians confers beneficial effects on SIRT6 protein function. centSIRT6 performed better at stimulating DNA repair, mitigating DNA damage, suppressing LINE1 transposons, and killing cancer cells. Rare genetic variants are more likely to be deleterious than beneficial (Nelson *et al*, 2012), and are often associated with human disease. The only other coding SIRT6 human mutation, which had been functionally characterized, leads to embryonic lethality (Ferrer *et al*, 2018). SIRT6 activity is highly correlated with aging and it has been demonstrated that overexpression of SIRT6 results in increased lifespan in mice (Kanfi *et al*, 2012; Roichman *et al*, 2021). It has also been reported that SIRT6 from long-lived species can confer increased longevity in *Drosophila* (Tian *et al*, 2019). Our findings indicate that increased SIRT6 activity has a beneficial impact on cellular functions linked to longevity and may contribute to increased lifespan in centenarians.

Genetic association tests on human extreme longevity are uniquely challenging given the rarity of individuals and the lack of reliable statistical power to detect small effects. To date, only two variants near APOE and FOXO3a have been associated with

longevity in genome-wide scans (Deelen *et al*, 2011; Broer *et al*, 2015). For FOXO3a, this required a large-scale meta-analysis involving 6,036 longevity cases and 3,757 controls (Broer *et al*, 2015). Since there simply are insufficiently large numbers of centenarians in human populations, the genetic association has limited utility in finding loci that promote healthy aging and longevity. In this study, we instead took a candidate SNP approach for *SIRT6* within a genetically isolated population of Ashkenazi Jews who exhibited extreme phenotype (>95 years old). The observed association for rs350845, which is linked to higher SIRT6 levels is nominally significant ($P = 0.049$). This association between higher SIRT6 expression and longevity is consistent with the data from *Drosophila* (Tian *et al*, 2019) and mouse (Kanfi *et al*, 2012) where SIRT6 overexpression resulted in lifespan extension. The missense variant centSIRT6 had twice the allele frequency in the AJ centenarians (1%) compared with controls (0.5%); however, we lacked the power to detect statistically significant differences ($P = 0.3$). To further validate this finding, a follow-up analysis of the GnomAD cohort of cohorts, which also contains AJ individuals, showed evidence of centSIRT6 enrichment among 75+ year-olds compared with all age groups. In addition to enrolling larger centenarian cohorts, future work may investigate epistasis and the co-occurrence of other SNPs in the genome with centSIRT6 and extreme longevity.

While increased SIRT6 activity correlates with a longer lifespan in model organisms (Kanfi *et al*, 2012; Tian *et al*, 2019), it has not been clear which of SIRT6's enzymatic activities are central to longevity. The seemingly contradictory nature of the centenarian SIRT6 allele possessing decreased deacetylase activity came as an unexpected result. SIRT6 KO mice show several progeroid phenotypes and do not typically survive past 30 days (Mostoslavsky *et al*, 2006). In these mice, both the deacetylase activity and ribosylase activity are abrogated. In this study, we have demonstrated that a centSIRT6 possesses reduced deacetylase activity *in vitro* and showed nondiscernable differences *in vivo*. The latter differences likely result from additional protein factors or PTMs present *in vivo* that help maintain SIRT6 deacetylation activity at close to the wild-type levels, despite the weakened core enzyme. Interestingly, loss of SIRT6 deacetylation activity in humans or SIRT6 knockout in monkeys lead to severe developmental phenotypes rather than premature aging, suggesting that, at least in primates, deacetylation activity of SIRT6 is required for development but not necessarily for adult longevity (Ferrer *et al*, 2018; Zhang *et al*, 2018).

The extent to which ADP-ribosylation functions of SIRT6 contribute to longevity remains largely unknown. Herein we report that the centSIRT6 allele displays significantly enhanced ribosylation activity against itself, PARP1 and KAP1 *in vitro* and also appeared enhanced *in vivo*. Further, we show that centSIRT6 confers improved aspects of SIRT6 function to living cells, including DNA DSB repair, LINE1 element suppression, and tumor cell suppression, all of which showed dependence on SIRT6 ADP-ribosylation functions previously. These results suggest that enhancement of ADP-ribosylation functions of SIRT6 contributes to increased longevity. While we cannot rule out that other aspects of SIRT6 activity, such as glucose metabolism and telomere maintenance, have been impacted by these mutations and may also play a role in the prolongevity functions of this allele, those effects have been largely attributed to SIRT6 deacetylase activity, which appears similar or

reduced compared with the WT allele. It remains possible that SIRT6 ADP ribosylation may play unanticipated roles in these processes as supported by recent reports of SIRT6 ADP ribosylation of SMARCA2 and KDM2A (Rezazadeh *et al*, 2019, 2020). Consistent with this idea, SIRT6 mono-ADP ribosylation (and subsequent activation) of PARP1 plays a critical role in DNA DSB repair by facilitating the recruitment of DNA repair proteins, such as MRN complex proteins (Haince *et al*, 2008; Van Meter *et al*, 2016). Improvements in DSB repair efficiency, specifically those driven by SIRT6 activity, have been shown to correlate with longevity and healthspan (Roichman *et al*, 2017; Tian *et al*, 2019). Additionally, the ribosylation of KAP1 by SIRT6 and subsequent recruitment to transposable elements plays a critical role in silencing these opportunistic elements, which have been linked to age-related sterile inflammation and DNA damage (Van Meter *et al*, 2014; De Cecco *et al*, 2019; Simon *et al*, 2019). These same elements have been linked to inflammation driven by senescent cells, which are prevalent in aged systems (De Cecco *et al*, 2019). Further investigation of the separation of function alleles of SIRT6 will be required to disentangle the contribution of its deacetylase/deacylase and ADP-ribosylation activities. Beyond its enhanced mADPr activity, centSIRT6 displays enhanced interaction with the nuclear scaffold protein LMNA. This result is especially significant for several reasons. LMNA functions as a key organizer of the nucleus, especially in maintaining heterochromatin at the nuclear periphery and LINE1 elements reside within lamina-associated domains (LADs) (Peric-Hupkes *et al*, 2010; Zullo *et al*, 2012). Aberrant processing of LMNA results in human premature aging syndrome, Hutchison Gilford Progeria, while LMNA SNPs have been identified in human centenarians (De Sandre-Giovannoli *et al*, 2003; Eriksson *et al*, 2003; Conneely *et al*, 2012). Fibroblasts isolated from centenarians were also shown to have increased levels of pre-LMNA, suggesting that modulated functions of LMNA are associated with both premature aging and exceptional longevity (Lattanzi *et al*, 2014; Ghosh *et al*, 2015) found that the catalytic domain of SIRT6 interacts with LMNA. In addition, they found that many key aspects of SIRT6 activity, such as PARP1 ribosylation and activation, as well as chromatin localization in response to DNA damage were lost in LMNA$^{-/-}$ MEFs. Our data suggest that a gain of function of SIRT6 may have the opposite effect of progerin on longevity. Remarkably, SNPs in LMNA were found in centenarians (Conneely *et al*, 2012). Fibroblasts isolated from centenarians were also shown to have increased levels of pre-LMNA, suggesting that modulated functions of LMNA are associated with both premature aging and exceptional longevity (Lattanzi *et al*, 2014).

Questions remain as to how centenarian SIRT6 allele together with LMNA enhances genome stability and contributes to longevity. As LMNA enhances SIRT6 enzymatic activities, the stronger interaction may result in higher SIRT6 activity (Ghosh *et al*, 2015). Additionally, centSIRT6 may enhance LMNA function through stronger binding or as a result of a differential interactome of ribosylated LMNA. Previous attempts to induce ribosylation of purified LMNA by SIRT6 *in vitro* have been unsuccessful, possibly due to the lack of PTMs and the 3D nuclear organization that may be necessary to shape the interaction between SIRT6 and LMNA. As ribosylations are notoriously difficult to detect by mass spectrometry, more work will need to be done to identify the specific residues on LMNA modified by SIRT6.
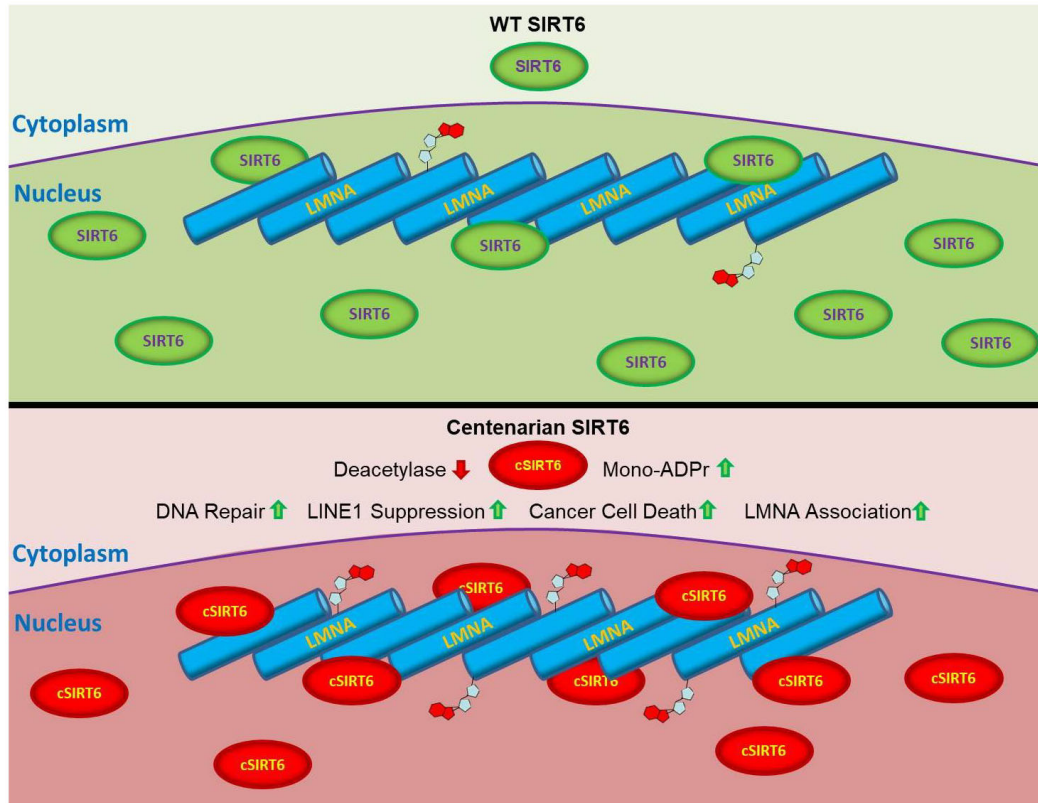
Figure 7. Altered molecular functions of centSIRT6.
CentSIRT6 allele shows reduced deacetylation activity and enhanced mADPr activity. This results in enhanced DNA repair, improved LINE1 suppression, and cancer cell killing. centSIRT6 shows stronger interaction with LMNA and enhances LMNA interactions with its partners.

In summary, we demonstrated that centSIRT6 displays reduced deacetylation activity *in vitro*, and has enhanced mADPr activity both *in vitro* and *in vivo*. This change in the balance of the two enzymatic activities leads to enhanced function of SIRT6 in DNA repair, LINE1 suppression, and cancer cell killing, which are the activities that require mADPr activity of SIRT6. centSIRT6 also shows enhanced binding to LMNA, which may further promote its function in DNA repair and chromatin organization via direct stimulation of SIRT6 enzymatic activity, and by coordinating interactions of LMNA with other components of LMNA complex (Fig 7). It would be interesting to model centSIRT6 in mice, to directly test whether this allele extends lifespan. However, the C-terminus of SIRT6 that harbors the centenarian mutations is not conserved in the mouse. SIRT6 and LMNA pathways are highly linked with the aging process, indicating that the SIRT6 ribosylation activity may be the more critical of the two enzymatic functions in regards to healthy aging and may aid LMNA to organize/control nuclear protein–protein and protein-RNA interactions. Given these results, there may be a benefit to enhancing SIRT6 activity, specifically the ribosylase activity. Molecules that impact SIRT6 activity, as well as its major co-enzyme NAD$^+$, have been identified and hold potential as future methods of anti-aging interventions (Li *et al*, 2017; Rahnasto-Rilla *et al*, 2018; Rajman *et al*, 2018). Further refining the search for interventions that specifically target the mADPr activity of SIRT6 may yield more specific therapeutics to improve lifespan and healthspan.

Materials and Methods

Human subjects

Ashkenazi Jewish population derived from an undetermined small number (estimated to be in the several thousands) of founders. External factors, including ecclesiastical edicts prohibiting all social contact with Jews, the Crusades, the establishment of the Pale of Settlement, numerous Pogroms, and ethnic bigotry, resulted in the social isolation and inbreeding of the Ashkenazi Jews. This history resulted in both cultural and genetic homogeneity and has made this population useful for the identification of genetic traits. In our study, a centenarian is defined as a healthy individual living independently at 95 years of age or older and control is defined as an individual without a family history of unusual longevity; parents of controls survived to the age of 85 years or less. The participants' ages were defined by birth certificates or dates of birth as stated on passports. This study group consisted of 450 Ashkenazi Jewish centenarians and 550 Ashkenazi Jewish controls that were previously collected as part of a longevity study at the Albert Einstein College of Medicine (Barzilai *et al*, 2003). The ages of centenarians were 100.4 ± 3.3 years (mean $\pm$ SD) and the ages of controls were 78.3 ± 8.1 years (mean $\pm$ SD) at the time of sequencing. 72% of centenarians and 52.55% of controls were female. The BMIs of centenarians were 26.9 ± 4.8 (mean $\pm$ SD) and the BMIs of controls

were 22.8 ± 3.6 (mean $\pm$ SD). Informed written consent was obtained in accordance with the policy of the committee on clinical investigations of the Albert Einstein College of Medicine, New York, NY. An additional 5,185 AJ controls were derived from GnomAD database.

Cell lines

HEK293 SIRT6 overexpression lines were generated by transfecting HEK293 cells with linearized CMV-SIRT6 plasmids via jetPRIME transfection reagent and selecting stably integrated clones. To generate normal human fibroblasts expressing WT and centenarian alleles of SIRT6 under the control of cumate-inducible promoter (cumate SIRT6 fibroblasts), constructs containing SIRT6 alleles under the control of cumate promoter were integrated into the genome of telomerase-immortalized SIRT6-KO human HCA2 foreskin fibroblasts via the PiggyBac Transposon Vector System. Endogenous SIRT6 was knocked out in these cells using CRISPR/Cas-9 (Tian *et al*, 2019). NHEJ and HR reporter assays were conducted using telomerase-immortalized HCA2 human fibroblast cell lines containing integrated reporter constructs (I9A and H15C) (Mao *et al*, 2008; Seluanov *et al*, 2010). HT1080 and HeLa cell lines were used to assess anti-tumor activity. Human H7 ESCs (WiCell Research) and their genetically modified derivatives were maintained on Matrigel in mTeSR Plus medium (Stem Cell Technology) and used to generate MSCs.

Cell culture

All cell lines were maintained in humidified incubators at 5% CO_2, 5% O_2, at 37°C. Cells were grown in Eagle's minimum essential medium with 15% fetal bovine serum and 1x penicillin/streptomycin, with the exception of the HEK293, HT1080, and HeLa cells, which were cultured in DMEM with D-Glucose and L-Glutamine. Human MSCs were cultured on Gelatin-coated plate in hMSC culture medium (αMEM (Gibco), 10% fetal bovine serum (GeminiBio), 1% penicillin/streptomycin (Gibco) and 1 ng/mL bFGF (ThermoFisher)). The cell lines are routinely tested for mycoplasma contamination.

Sequencing of *SIRT6* gene in Ashkenazi Jewish Centenarians

The sequencing of SIRT6 gene was a part of the pooled target capture sequencing (capture-seq) project aiming to discover centenarian-enriched rare variants in genes involved in conserved longevity assurance pathways (Ryu *et al*, 2018). SIRT6 was selected as a candidate longevity-associated gene. All SIRT6 variants discovered in the capture-seq of 1,000 AJ samples (450 centenarians vs. 550 controls) are provided in Table 1.

Plots of *SIRT6* expression and eQTL status for rs350845 were downloaded from the GTEx website.

GnomAD *centSIRT6* enrichment

GnomAD analysis was performed on the 2.1.1 release of combined exome and whole-genome sequences representing 125,748 exomes and 15,708 whole genomes. Chromosome 19 variants were downloaded from the GnomAD database, and since the centSIRT6 allele

is rare (0.5% - 1%) we filtered for SNPs between 0.1% and 1% frequency. Our goal was to build a distribution of allele occupancy in the 75+ age group normalized against all age groups. While this is not a traditional association study *per se*, it does allow us to witness allele frequency bias in older vs. younger age brackets.

$$Normalized\ over75\ allele\ counts = \frac{allele\ counts\ in\ over75}{allele\ counts\ all\ ages}$$

A normalized value of 0 represents a complete absence of the allele in 75+, and higher values represent greater occupancy of that allele in the 75+ age bracket compared with all ages. Alleles with a value of 1 were filtered from consideration, as these may have represented alleles only observed in cohorts comprised of older individuals. In total 66,441 SNPs were measured, of which 3,307 were missense.

Gene editing at SIRT6 locus

CRISPR/Cas9-mediated knock-in was performed using Alt-R CRISPR-Cas9 System (IDT) and HDR Donor Oligos. Cas9 nuclease, sgRNA (GAATCTCCCACCCGGATCAA) targeting double variant site and single-strand DNA oligo donors (ssODNs) containing SIRT6 double variant were ordered from IDT. To generate SIRT6 double variant knock-in hESCs, 2×10^5 individualized hESCs were resuspended in 10 μL Resuspension Buffer R (Invitrogen) containing CRISPR ribonucleoproteins (Cas9 protein + sgRNA) and ssODNs and were then electroporated using NEON Transfection System (Invitrogen). After electroporation, cells were seeded on Matrigel-coated plates in mTeSR Plus with 1x RevitaCell Supplement (Gibco). After 48 h expansion, cells were dissociated by Accutase and 10,000 cells were seeded on CytoSort™ Array (10,000 microwells, CELL Microsystem). Once cells were attached, microwells containing a single colony were automatically picked and transferred to a 96-well plate by CellRaft AIR System (CELL Microsystem). The expanded clones on a 96-well plate were further genotyped by TaqMan genotyping assay (rs201141490, rs183444295, ThermoFisher) and Sanger sequencing.

MSC differentiation

hESCs-derived embryoid bodies were first produced using Aggre-Well (Stem Cell technology) and were then plated on Matrigel-coated plates in hMSC differentiation medium (αMEM (Gibco), 10% fetal bovine serum (GeminiBio), 1% penicillin/streptomycin (Gibco), 10 ng/mL bFGF (ThermoFisher) and 5 ng/mL TGFβ (Thermofisher)) for around 10 days till fibroblast-like cells were confluent. These fibroblast-like cells were maintained in an hMSC culture medium on Gelatin-coated 10 cm dishes for two passages and were further sorted by FACS machine (BD FACS Aria II) to purify CD73/CD90/CD105 tri-positive hMSCs.

Western blotting

Cells and reactions were collected using a 2x Laemmli solution and incubated on ice for 15 min, during which time the samples were passed through a large gauge needle several times and vortexed every 5 min. Samples were then spun at 14,000 RPM to remove

debris, and the supernatant was transferred to a new tube. Samples were heated in boiling water for 20 min before being centrifuged at 14,000 RPM for 1 min and loaded into a BioRad Criterion 4–20% gel. After transfer to PDVF membrane and blocked (5% dehydrated milk) for 2 h at RT, membranes were incubated overnight antibodies in 2.5% blocking buffer at 4°C. Membranes were washed 3x with TBST for 10 min each before secondary antibody in 1x TBST was added for 2 h incubation at RT. Membranes were washed 3x with TBST for 10 min and then imaged.

The following antibodies were used: H3 (Abcam ab500)-1:5,000, H3K9ac (Abcam ab4441)-1:1,000, H3K18ac (Abcam ab1191)-1:1,000, β-tubulin (Abcam ab6046)-1:10,000, SIRT6 (Cell Signaling #12486)-1:1,000, Lamin A/C-1:1,000 (Abcam ab108595, Millipore 05–714), γH2AX (Millipore 05–636), PARP1(Abcam ab227244)-1:1,000, Vimentin-1:1,000 (Abcam ab92547); TAF15-1:2,000 (Abcam ab134916); mADPr 1:500 (AbD33204 and AbD33205)(Bonfiglio et al, 2020).

Immunoprecipitation

Cells were plated and grown with equivalent dosages of cumate for 48 h prior to IP. In brief, cells were collected via trypsin and centrifugation and then lysed on ice using IP Buffer (20 mM HEPES pH = 8, 0.2 mM EDTA, 5% glycerol, 150 mM NaCl, 1% NP40) + COMplete protease inhibitor for 10 min. The lysate was sonicated at 25% output for 10 pulses, and then, debris was pelleted by centrifugation at 4°C at 13,000 RPM for 10 min. Supernatant was transferred to a new tube and precleared with A/G Sepharose beads at 4°C for 1 h on a rotator. Beads were removed by centrifugation and transfer of cleared sample to new tubes. 50 µl of the sample was reserved as input control. Samples were incubated overnight at 4°C with 3 µg of antibody (SIRT6-Cell Signaling #12486; PARP1-Abcam ab227244; Lamin A/C-Millipore 05–714; Vimentin-Abcam ab92547; TAF15-Abcam ab134916; AbD33204(Bonfiglio et al, 2020), AbD33205(Bonfiglio et al, 2020), then with 30 µl of 25% Sepharose for 2 h at 4°C. Samples were spun down, and beads were washed 5x with IP buffer. Final resuspension with 100 µl IP buffer.

DNA repair assays

Both NHEJ and HR efficiency were assessed as previously described (Seluanov et al, 2010). In brief, I-Sce1, SIRT6 or HPRT control, and DsRed plasmid were transfected into telomerase-immortalized human foreskin fibroblasts containing chromosomally integrated NHEJ or HR reporter cassettes (I9A or H15C) cells (Mao et al, 2008). Cells were allowed 3 days to recover prior to analysis by flow cytometry. 20,000 live cells were gated and assessed for each transfected population. Efficiency was calculated as the ratio of GFP events over DsRed events.

Transfections

Transfections were carried out by plating cells at a density of 500,000 cells/10 cm plate two days prior to transfection. Transfections were carried out using the Amaxa Nucleofector with Normal Human Dermal Fibroblast transfection solution following the manufacturer's protocol. For cancer cell transfections, jetPRIME transfection reagent was used to deliver plasmids into cells.

Quantitative RT–PCR

Total RNA was isolated from cells at 80% confluence using Trizol Reagent and then treated with DNase. cDNA was synthesized using Superscript III (Life Technologies) cDNA kit with the OligodT primer. qRT–PCR was performed on the BioRad CFX Connect Real-Time machine with SYBR Green Master Mix (BioRad) using 30 ng of cDNA per reaction with 3x reactions/sample. All primer sets were tested for specificity and efficiency targeting the human L1PA1 evolutionary active family of LINE1 elements. Actin was assayed using QuantumRNA Actin Universal primers (Thermo AM1720). For NRF2 pathway gene expression, total RNA was isolated from cells using RNeasy Plus Mini Kit (QIAGEN). cDNA was synthesized using PrimeScript RT Master Mix (Takara). qRT–PCR was performed with PowerUp SYBR Green Master Mix (Thermofisher) in QuantStudio 6 Pro Real-Time PCR System (Thermofisher). All primer sets were tested for specificity and efficiency. hLINE1 ORF1 Fwd-GTTCCTC ACCAGCAACAGAACAA, Rev-GTTTGAATGTCCTCCCGTAGCTC; hLINE1 ORF2 Fwd-GCAGGGGTTGCAATCCTAGTC, Rev- CTGGGTGCTCCT GTATTGGGT; 18S Fwd-GTAACCCGTTGAACCCCATT, Rev-CCATCC AATCGGTAGTAGCG; NRF2 Fwd-TCAGCGACGGAAAGAGTATGA, Rev-CCACTGGTTTCTGACTGGATGT; NQO1 Fwd-CGCAGACCTTG TGATATTCCAG, Rev-CGTTTCTTCCATCCTTCCAGG; HO-1 Fwd-AA GACTGCGTTCCTGCTCAAC, Rev-AAAGCCCTACAGCAACTGTCG; GCLC Fwd-GGATTTGGAAATGGGCAATTG, Rev-CTCAGATATACT GCAGGCTTGGAA; GCLM Fwd-TGCAGTTGACATGGCCTGTT, Rev-TCACAGAATCCAGCTGTGCAA.

Immunofluorescence and apoptosis

γH2AX and 53BP1 immunostaining was carried out as previously described(Mao et al, 2011). Anti- γH2AX (05–636) and anti-53BP1 (MAB3804) antibodies were purchased from Millipore. Apoptosis in fibroblasts was measured using the Annexin V Staining Kit (Roche).

MMS treatment

3×10^4 hMSCs were seeded on a gelatin-coated 96-well plate and hMSCs were treated with DNA-damaging agents for 48 h upon reaching 90% confluence. CellTiter 96 AQueous One Solution Cell Proliferation Kit (MTS assay, Promega) was used to measure cell viability according to the manufacturer's protocol. DNA-damaging agents employed in this assay were as follows: Methyl methanesulfonate (0.125/0.25/0.5 mM, MMS).

Gamma irradiation

Cells were grown to 75% confluency prior to treatment on coated slides. A Cs-137 irradiator was used to deliver 2Gy of radiation to cells. Cells were transported in a 37°C container and media was replaced postexposure.

Paraquat treatment

Cells were maintained to 75% confluency, at which point fresh media lacking sodium pyruvate and containing paraquat was added. Cells were maintained for 24 h in treated media, followed by

replacement with fresh media lacking sodium pyruvate. 48 h post-treatment, the cells were stained and evaluated for apoptosis.

SIRT6 protein purification

His-tagged SIRT6 cDNA was cloned into pET11a vectors and transformed into Rosetta-Gami *E. coli* cells. Cells were grown in presence of antibiotics and then protein production was induced with 0.5 mM IPTG 2 h before harvest. Cells were spun down and lysed on ice for 1 h using a solution of 50 mM Tris–HCl (pH = 7.5), 300 mM NaCl, 10% glycerol, and 10 mM imidazole with EDTA-free protease inhibitor (Sigma #P8849) and 1 mg/ml egg white lysozyme followed by sonication with a Branson instrument. After the removal of cell debris by centrifugation, the lysate was incubated with Ni_2^+ -NTA agarose overnight. Solution with beads was placed in gravity column and washed with lysis solution, followed by 2 volumes of wash buffer (lysis buffer + 30 mM imidazole). Finally, the protein was eluted with elution buffer (lysis buffer + 500 mM imidazole) and fractions were collected. Protein concentration was assessed by BCA assay and run on an SDS–PAGE gel. The 3–4 highest concentration fractions were pooled and dialyzed against storage buffer (50 mM Tris–HCl pH = 7.5, 150 mM NaCl, 1 mM DTT, 5% glycerol).

Stable Isotope Labeling of Amino Acids in Cell Culture (SILAC)

Turnover experiments were performed using HEK293 cell lines stably expressing SIRT6 WT or centSIRT6. Cells were cultured for one week until confluent in MEM for SILAC (Thermo) supplemented with 10% dialyzed FBS (Gibco), L-glutamine, L-arginine $^{13}C_6$ $^{15}N_4$ (Cambridge Isotopes), and L-lysine $^{13}C_6$ $^{15}N_2$ (Cambridge Isotopes). The media was changed to a normal culture medium, and cell pellets were harvested at 0, 2, 4, 6, 8, 12, and 24 h postmedia change. Cell pellets were lysed in buffer containing 8 M urea, 75 mM NaCl, 50 mM Tris, pH 8.5, with a protease inhibitor cocktail (Roche). Pellets were vortexed for 30s and sonicated 5x 10 s with 1 min rest on ice in between sonication steps. The lysate was centrifuged at 15,000 xg for 10 min, and then, the supernatant was collected.

SIRT6 deacylation activity

The substrate for this reaction is a synthetic TNF-derived peptide first developed by Schuster *et al* (2016) was synthesized by Genscript. Reactions were performed with 150 mM NaCl, 20 mM Tris, 5% glycerol, 1 mM β-mercaptoethanol, 2 µM SIRT6, and substrate concentration ranges of 7–1,000 µM NAD^+ and 2–88 µM peptide. Reactions were performed at 37°C and fluorescence was measured using 310/405 nm excitation/emission spectra on a Tecan Spark 20 M plate reader. Readings were taken every 30s and initial rates were calculated from the relative fluorescence increase over a minimum of 6 min.

Histone analysis

Histones were purified from cumate SIRT6 fibroblasts (SIRT6 KO primary human foreskin fibroblasts constitutively expressing the catalytic subunit of telomerase and various alleles of SIRT6 via a cumate-inducible promoter) using an established acid extraction method followed by propionylation of lysines prior to trypsin digestion to enhance coverage (Shechter *et al*, 2007; Sidoli *et al*, 2016). A data-independent analysis (DIA) mass spectrometry (MS) method was employed for quantitation of modified peptides after samples were separated by nano-LC using EpiProfile (Sidoli *et al*, 2015) or, alternatively, after direct infusion followed by a one-minute acquisition and analysis with EpiProfileLite (Sidoli *et al*, 2019).

Analysis of SIRT6 and LMNA protein–protein interactions by mass spec

Cumate SIRT6 fibroblasts were used to compare interactomes for centSIRT6 and the wild-type SIRT6. Nuclear extracts were prepared using a hypotonic lysis buffer. Nuclei isolated from approximately 2.5×10^7 cells were resuspended in one ml of extraction buffer (50 mM Tris–HCl pH 7.5, 150 mM NaCl, 10% glycerol, 5 mM DTT, 0.25% NP-0.4, 1x Roche Complete protease inhibitors, as well as kinase/phosphatase inhibitors—1 mM NaVO4, 10 mM beta-glycerophosphate, 1 mM sodium pyrophosphate, 1 mM NaF), and nuclei were disrupted by passage through a 27 gauge needle followed by sonication (3 pulses at constant 20% power) with a Branson Sonifier on ice. Next, samples were filtered through a 0.2 µm MWCO filter to remove any insoluble material (and reduce nonspecific binding). Proteins were quantified using the BCA assay, and equal amounts of wild-type SIRT6 and centSIRT6-derived extract were divided into 5 replicates each. Three replicates of extract received 4 µg of anti-SIRT6 antibody (Cell Signaling #1248) or anti-Lamin A (Lamin A/C-Millipore 05–714) and 75 µl of Miltenyi protein G µMACS magnetic particles. Two of the replicates were mixed with normal rabbit IgG (Cell Signaling #2729) as controls for nonspecific binding to the particles. Samples were rotated at 4°C for 6 h followed by separation by the magnet. Samples were washed with 3 additional ml of extraction buffer and eluted with 100 µl of boiling elution buffer (5% SDS with 50 mM Tris–HCl pH 7.5). After removal of SDS with S-columns (Protifi; Huntington, NY) and trypsin digestion, peptides were resuspended in MS-grade water and labeled with tandem mass tags (TMT 10-plex; Thermo Fisher). Samples were resolved by nano-electrospray ionization on an Orbitrap Fusion Lumos MS instrument (Thermo) in positive ion mode using a 30 cm homemade column packed with 1.8 µm C-18 beads to resolve the peptides. Solvent A was 0.1% formic acid and solvent B was 100% acetonitrile (CAN) with 0.1% formic acid. The length of the run was 2 h with a 90 min gradient. CID (35% collision energy) was used for MS2 fragmentation. HCD (60% collision energy) was used for MS3 detection of TMT groups. Other details of the run parameters may be found in the embedded run report of the RAW data file uploaded to the ProteomeXchange database. Peptide assignments were made using Proteome Discoverer and Sequest and MS3 ions were used for quantitation. False discovery rates (FDR) were estimated using a Decoy Database Search with Target FDR (strict) set to 0.01 and Target FDR (relaxed) set to 0.05. Validation was based on q-value. In the consensus step, ions with a co-isolation threshold above 30% were excluded. Normalization between replicates was achieved using the total protein approach (Wisniewski, 2017) where peptide counts for a single protein were divided by the sum of all proteins in the lane. Proteins appearing in specific antibodies (either anti-SIRT6 or anti-Lamin A) compared with normal IgG serum with

the Student's *t*-test $P < 0.05$) were considered as interactions. Similarly, proteins showing higher levels in centSIRT6 versus wild-type SIRT6 were based upon $P < 0.05$.

SIRT6-NAD$^+$ binding by tryptophan fluorescence

One µM of SIRT6 protein in 50 µl of buffer (50 mM Tris–HCl pH = 7.5 and 150 mM NaCl) was combined with a range of NAD$^+$ (0–2 mM). Samples were then placed in a 384 Corning Flat Black plate and analyzed in a Tecan Spark 20 M plate reader. Fluorescence was measured across the 300–400 nm range in 2 nm steps using a 280 nm excitation. Background quenching by NAD$^+$ of SIRT6 denatured by 7 M urea was subtracted from the spectra as described previously (Pan *et al*, 2011).

Deacetylase Assay

Three µg of SIRT6 protein was combined with 0.5 µg histones, 1 or 5 mM NAD$^+$, 30 mM Tris–HCl pH = 8, 4 mM MgCl$_2$, 1 mM DTT and ddH$_2$O up to 50 µl. Designer nucleosomes with relevant PTMs were obtained from Epicypher. Common reagents were prepared as a master mix prior to the addition of SIRT6 protein. All reagents were prepared on ice and moved to 37°C for the duration of the incubation. The reaction was quenched with direct application of 1 volume of 2x Laemmli buffer with BME. Samples were boiled for 15 min before being run in Western analysis using anti-H3K9ac and anti-H3K18ac antibodies.

PARP1 Ribosylation Assay

Five µg of SIRT6 protein was combined with 100 fm PARP1, 20 mM Tris–HCl pH = 8, 10 µM ZnCl$_2$, 10 µM MgCl$_2$, 10% glycerol, 300 µM NAD$^+$, 1 mM DTT, 0.1 µg/ml salmon sperm DNA and ddH$_2$O up to 50 µl. All reagents were prepared on ice as a master mix and moved to 30°C for 30 min upon addition of SIRT6. The reaction was quenched with direct application of 1 volume of 2x Laemmli buffer with BME. Samples were boiled for 15 min before being run in Western analysis using anti-PADPR antibody (Abcam Ab14459).

KAP1 Ribosylation Assay

KAP1 ribosylation was conducted using the protocol in Van Meter *et al*, 2014, with Biotin-NAD$^+$ (Tocris 6,573) in leu of [^{32}P] NAD$^+$. Five µg of KAP1 protein was used in each reaction. Reactions were prepared as a master mix prior to the addition of SIRT6. Samples were boiled and then run on SDS–PAGE gel and then transferred to PDPF membrane. Membranes were probed using HRP streptavidin (Sigma RABHRP3)

SIRT6 Ribosylation Assay

Three µg of SIRT6 was combined with 50 mM Tris–HCl pH = 7.5, 1 mM DTT, 10 µM ZnCl$_2$, 150 mM NaCl, 25uM Biotin-NAD$^+$ (Tocris 6,573), and ddH$_2$O up to 20 µl. All reagents were combined on ice in a master mix except for SIRT6. Master mix was aliquoted into reaction tubes and SIRT6 was added and incubated at 37°C for 3 h. The reaction was quenched with 1 volume of 2x Laemmli buffer with BME. Samples were boiled and then run on SDS–PAGE gel and

then transferred to PDPF membrane. Membranes were probed using HRP-streptavidin (Sigma RABHRP3).

Chromatin Immunoprecipitation (ChIP)

Cells were harvested at 80% confluency after 48 h with or without cumate. Trypsin was used to remove cells from the plate and then neutralized with PBS containing FBS and spun down to collect the cell pellet. The cell pellet was washed with cold PBS 1x prior to using Abcam Ab500 ChIP Kit. H3K9ac (Abcam ab4441), H3K18ac (Abcam ab1191), and SIRT6 (Cell Signaling #12486) antibodies were used. The manufacturer's protocol was used with the following considerations: Fixation time = 10 min at 37°C, Sonication settings (Qsonica Instrument) = 12.5 min, 15 s on/off, 30% output, 4°. qPCR primers from (Kawahara *et al*, 2009; Tasselli *et al*, 2016) were used.

Thermostability

Four µM SIRT6 protein was combined with 1x SYPRO Orange dye in storage buffer (50 mM Tris–HCl pH = 7.5, 150 mM NaCl, 1 mM DTT, 5% glycerol) to 50 µl. Samples were placed in a qRT–PCR plate and run on a BioRad CFX Connect Real-Time machine using a Melt Curve protocol (30°C-75°C, 0.5°C steps in 10 s intervals).

Statistics

Unless otherwise noted, the Student's *t*-test was used to determine statistical significance between groups. All tests were two-tailed and *P*-values were considered significant below a 0.05 threshold. For two-way ANOVA tests, a Bonferroni correction was applied. Cell culture experiments utilized at least two separately derived cell lines for each genotype and were performed in triplicate unless noted otherwise. *In vitro* assays were done in triplicate using two or more separate protein isolation preps. Blinding was not conducted for assays.

Data availability

All sequencing data have been deposited in the Sequence Read Archive (SRA) under the bioproject number

- Sequencing data, DNA damage genes PRJNA669033 (https://www.ncbi.nlm.nih.gov/bioproject/PRJNA669033/),
- Capture-seq data, Sequence Read Archive PRJNA669034 (https://www.ncbi.nlm.nih.gov/bioproject/?term = PRJNA669034)
- RNAseq data, Sequence Read Archive PRJNA862192 (https://www.ncbi.nlm.nih.gov/bioproject/PRJNA862192)
- The mass spectrometry proteomics data have been deposited to the ProteomeXchange Consortium via the PRIDE [1] partner repository with the dataset identifier PXD035689 and 10.6019/PXD035689

Expanded View for this article is available online.

Author contributions

Matthew Simon: Conceptualization; formal analysis; investigation; visualization; methodology; writing—original draft; writing—review and editing. **Jiping Yang:** Investigation. **Jonathan Gigas:** Investigation. **Eric J Earley:** Investigation. **Eric Hillpot:** Investigation. **Lei Zhang:** Investigation. **Maria Zagorulya:** Investigation. **Greg Trombline:** Investigation. **Michael Gilbert:** Investigation. **Samantha L Yuen:** Investigation. **Alexis Pope:** Investigation. **Michael Van Meter:** Investigation. **Stephan Emmrich:** Investigation. **Denis Firsanov:** Investigation. **Advait Athreya:** Investigation. **Seyed Ali Biashad:** Investigation. **Jeehae Han:** Investigation. **Seungjin Ryu:** Investigation. **Archana Tare:** Investigation. **Yizhou Zhu:** Investigation. **Adam Hudgins:** Investigation. **Gil Atzmon:** Investigation. **Nir Barzilai:** Investigation. **Aaron Wolfe:** Investigation. **Kelsey Moody:** Investigation. **Benjamin A Garcia:** Funding acquisition; investigation. **David D Thomas:** Investigation. **Paul D Robbins:** Funding acquisition; investigation. **Jan Vijg:** Writing—review and editing. **Andrei Seluanov:** Conceptualization; resources; supervision; funding acquisition; validation; visualization; methodology; project administration; writing—review and editing. **Yousin Suh:** Conceptualization; resources; funding acquisition; visualization; methodology; project administration; writing—review and editing. **Vera Gorbunova:** Conceptualization; resources; supervision; funding acquisition; validation; visualization; methodology; project administration; writing—review and editing.

Disclosure and competing interests statement

VG serves on the SAB of Genflow and DoNotAge. Other authors declare no competing interests or other interests that might be perceived to influence the results and/or discussion reported in this paper.

References

Adolph KW (1987) ADPribosylation of nuclear proteins labeled with [3H] adenosine: changes during the HeLa cycle. *Biochim Biophys Acta* 909: 222–230

Adolph KW, Song MK (1985) Variations in ADP-ribosylation of nuclear scaffold proteins during the HeLa cell cycle. *Biochem Biophys Res Commun* 126: 840–847

Barzilai N, Atzmon G, Schechter C, Schaefer EJ, Cupples AL, Lipton R, Cheng S, Shuldiner AR (2003) Unique lipoprotein phenotype and genotype associated with exceptional longevity. *JAMA* 290: 2030–2040

Beli P, Lukashchuk N, Wagner SA, Weinert BT, Olsen JV, Baskcomb L, Mann M, Jackson SP, Choudhary C (2012) Proteomic investigations reveal a role for RNA processing factor THRAP3 in the DNA damage response. *Mol Cell* 46: 212–225

Bilan V, Leutert M, Nanni P, Panse C, Hottiger MO (2017) Combining higher-energy collision dissociation and electron-transfer/higher-energy collision dissociation fragmentation in a product-dependent manner confidently assigns proteomewide ADP-ribose acceptor sites. *Anal Chem* 89: 1523–1530

Bonfiglio JJ, Leidecker O, Dauben H, Longarini EJ, Colby T, San Segundo-Acosta P, Perez KA, Matic I (2020) An HPF1/PARP1-based chemical biology strategy for exploring ADP-ribosylation. *Cell* 183: 1086–1102

Broer L, Buchman AS, Deelen J, Evans DS, Faul JD, Lunetta KL, Sebastiani P, Smith JA, Smith AV, Tanaka T *et al* (2015) GWAS of longevity in CHARGE consortium confirms APOE and FOXO3 candidacy. *J Gerontol A Biol Sci Med Sci* 70: 110–118

Conneely KN, Capell BC, Erdos MR, Sebastiani P, Solovieff N, Swift AJ, Baldwin CT, Budagov T, Barzilai N, Atzmon G *et al* (2012) Human longevity and common variations in the LMNA gene: a meta-analysis. *Aging Cell* 11: 475–481

De Cecco M, Ito T, Petrashen AP, Elias AE, Skvir NJ, Criscione SW, Caligiana A, Brocculi G, Adney EM, Boeke JD *et al* (2019) L1 drives IFN in senescent cells and promotes age-associated inflammation. *Nature* 566: 73–78

De Sandre-Giovannoli A, Bernard R, Cau P, Navarro C, Amiel J, Boccaccio I, Lyonnet S, Stewart CL, Munnich A, Le Merrer M *et al* (2003) Lamin a truncation in Hutchinson-Gilford progeria. *Science* 300: 2055

Deelen J, Beekman M, Uh HW, Helmer Q, Kuningas M, Christiansen L, Kremer D, van der Breggen R, Suchiman HE, Lakenberg N *et al* (2011) Genome-wide association study identifies a single major locus contributing to survival into old age; the APOE locus revisited. *Aging Cell* 10: 686–698

Eriksson M, Brown WT, Gordon LB, Glynn MW, Singer J, Scott L, Erdos MR, Robbins CM, Moses TY, Berglund P *et al* (2003) Recurrent de novo point mutations in lamin A cause Hutchinson-Gilford progeria syndrome. *Nature* 423: 293–298

Etchegaray JP, Mostoslavsky R (2015) Cell Fate by SIRT6 and TETs. *Cell Cycle* 14: 2187–2188

Ferrer CM, Alders M, Postma AV, Park S, Klein MA, Cetinbas M, Pajkrt E, Glas A, van Koningsbruggen S, Christoffels VM *et al* (2018) An inactivating mutation in the histone deacetylase SIRT6 causes human perinatal lethality. *Genes Dev* 32: 373–388

Ghosh S, Liu B, Wang Y, Hao Q, Zhou Z (2015) Lamin A is an endogenous SIRT6 activator and promotes SIRT6-mediated DNA repair. *Cell Rep* 13: 1396–1406

Gioutlakis A, Klapa MI, Moschonas NK (2017) PICKLE 2.0: a human protein-protein interaction meta-database employing data integration via genetic information ontology. *PLoS One* 12: e0186039

Haince JF, McDonald D, Rodrigue A, Dery U, Masson JY, Hendzel MJ, Poirier GG (2008) PARP1-dependent kinetics of recruitment of MRE11 and NBS1 proteins to multiple DNA damage sites. *J Biol Chem* 283: 1197–1208

Hendriks IA, Larsen SC, Nielsen ML (2019) An advanced strategy for comprehensive profiling of ADP-ribosylation sites using mass spectrometry-based proteomics. *Mol Cell Proteomics* 18: 1010–1026

Hirvonen K, Laivuori H, Lahti J, Strandberg T, Eriksson JG, Hackman P (2017) SIRT6 polymorphism rs117385980 is associated with longevity and healthy aging in Finnish men. *BMC Med Genet* 18: 41

Huttlin EL, Ting L, Bruckner RJ, Gebreab F, Gygi MP, Szpyt J, Tam S, Zarraga G, Colby G, Baltier K *et al* (2015) The BioPlex network: a systematic exploration of the human interactome. *Cell* 162: 425–440

Jiang H, Khan S, Wang Y, Charron G, He B, Sebastian C, Du J, Kim R, Ge E, Mostoslavsky R *et al* (2013) SIRT6 regulates TNF-alpha secretion through hydrolysis of long-chain fatty acyl lysine. *Nature* 496: 110–113

Jungmichel S, Rosenthal F, Altmeyer M, Lukas J, Hottiger MO, Nielsen ML (2013) Proteome-wide identification of poly(ADP-Ribosyl)ation targets in different genotoxic stress responses. *Mol Cell* 52: 272–285

Kaidi A, Weinert BT, Choudhary C, Jackson SP (2010) Human SIRT6 promotes DNA end resection through CtIP deacetylation. *Science* 329: 1348–1353

Kanfi Y, Naiman S, Amir G, Peshti V, Zinman G, Nahum L, Bar-Joseph Z, Cohen HY (2012) The sirtuin SIRT6 regulates lifespan in male mice. *Nature* 483: 218–221

Kawahara TL, Michishita E, Adler AS, Damian M, Berber E, Lin M, McCord RA, Ongaigui KC, Boxer LD, Chang HY *et al* (2009) SIRT6 links histone H3 lysine 9 deacetylation to NF-kappaB-dependent gene expression and organismal life span. *Cell* 136: 62–74

Kawahara TL, Rapicavoli NA, Wu AR, Qu K, Quake SR, Chang HY (2011) Dynamic chromatin localization of Sirt6 shapes stress- and aging-related transcriptional networks. *PLoS Genet* 7: e1002153

Lattanzi G, Ortolani M, Columbaro M, Prencipe S, Mattioli E, Lanzarini C, Maraldi NM, Cenni V, Garagnani P, Salvioli S *et al* (2014) Lamins are rapamycin targets that impact human longevity: a study in centenarians. *J Cell Sci* 127: 147–157

Leslie Pedrioli DM, Leutert M, Bilan V, Nowak K, Gunasekera K, Ferrari E, Imhof R, Malmstrom L, Hottiger MO (2018) Comprehensive ADP-ribosylome analysis identifies tyrosine as an ADP-ribose acceptor site. *EMBO Rep* 19: e45310

Li J, Bonkowski MS, Moniot S, Zhang D, Hubbard BP, Ling AJ, Rajman LA, Qin B, Lou Z, Gorbunova V *et al* (2017) A conserved NAD(+) binding pocket that regulates protein-protein interactions during aging. *Science* 355: 1312–1317

Li Y, Qin J, Wei X, Liang G, Shi L, Jiang M, Xia T, Liang X, He M, Zhang Z (2016) Association of SIRT6 gene polymorphisms with human longevity. *Iran J Public Health* 45: 1420–1426

Mao Z, Bozzella M, Seluanov A, Gorbunova V (2008) Comparison of nonhomologous end joining and homologous recombination in human cells. *DNA Repair (Amst)* 7: 1765–1771

Mao Z, Hine C, Tian X, Van Meter M, Au M, Vaidya A, Seluanov A, Gorbunova V (2011) SIRT6 promotes DNA repair under stress by activating PARP1. *Science* 332: 1443–1446

Martello R, Leutert M, Jungmichel S, Bilan V, Larsen SC, Young C, Hottiger MO, Nielsen ML (2016) Proteome-wide identification of the endogenous ADP-ribosylome of mammalian cells and tissue. *Nat Commun* 7: 12917

Michishita E, McCord RA, Berber E, Kioi M, Padilla-Nash H, Damian M, Cheung P, Kusumoto R, Kawahara TL, Barrett JC *et al* (2008) SIRT6 is a histone H3 lysine 9 deacetylase that modulates telomeric chromatin. *Nature* 452: 492–496

Min L, Ji Y, Bakiri L, Qiu Z, Cen J, Chen X, Chen L, Scheuch H, Zheng H, Qin L *et al* (2012) Liver cancer initiation is controlled by AP-1 through SIRT6-dependent inhibition of survivin. *Nat Cell Biol* 14: 1203–1211

Montecucco A, Biamonti G (2013) Pre-mRNA processing factors meet the DNA damage response. *Front Genet* 4: 102

Mostoslavsky R, Chua KF, Lombard DB, Pang WW, Fischer MR, Gellon L, Liu P, Mostoslavsky G, Franco S, Murphy MM *et al* (2006) Genomic instability and aging-like phenotype in the absence of mammalian SIRT6. *Cell* 124: 315–329

Naro C, Bielli P, Pagliarini V, Sette C (2015) The interplay between DNA damage response and RNA processing: the unexpected role of splicing factors as gatekeepers of genome stability. *Front Genet* 6: 142

Nelson MR, Wegmann D, Ehm MG, Kessner D, St Jean P, Verzilli C, Shen J, Tang Z, Bacanu SA, Fraser D *et al* (2012) An abundance of rare functional variants in 202 drug target genes sequenced in 14,002 people. *Science* 337: 100–104

Oughtred R, Stark C, Breitkreutz BJ, Rust J, Boucher L, Chang C, Kolas N, O'Donnell L, Leung G, McAdam R *et al* (2019) The BioGRID interaction database: 2019 update. *Nucleic Acids Res* 47: D529–D541

Pan CP, Muino PL, Barkley MD, Callis PR (2011) Correlation of tryptophan fluorescence spectral shifts and lifetimes arising directly from heterogeneous environment. *J Phys Chem B* 115: 3245–3253

Pan H, Guan D, Liu X, Li J, Wang L, Wu J, Zhou J, Zhang W, Ren R, Zhang W *et al* (2016) SIRT6 safeguards human mesenchymal stem cells from oxidative stress by coactivating NRF2. *Cell Res* 26: 190–205

Patil A, Nakamura H (2005) HINT: a database of annotated protein-protein interactions and their homologs. *Biophysics (Nagoya-shi)* 1: 21–24

Peric-Hupkes D, Meuleman W, Pagie L, Bruggeman SW, Solovei I, Brugman W, Graf S, Flicek P, Kerkhoven RM, van Lohuizen M *et al* (2010) Molecular maps of the reorganization of genome-nuclear lamina interactions during differentiation. *Mol Cell* 38: 603–613

Rahnasto-Rilla M, Tyni J, Huovinen M, Jarho E, Kulikowicz T, Ravichandran S, A Bohr V, Ferrucci L, Lahtela-Kakkonen M, Moaddel R (2018) Natural polyphenols as sirtuin 6 modulators. *Sci Rep* 8: 4163

Rajman L, Chwalek K, Sinclair DA (2018) Therapeutic potential of NAD-boosting molecules: the *in vivo* evidence. *Cell Metab* 27: 529–547

Rezazadeh S, Yang D, Biashad SA, Firsanov D, Takasugi M, Gilbert M, Tombline G, Bhanu NV, Garcia BA, Seluanov A *et al* (2020) SIRT6 mono-ADP ribosylates KDM2A to locally increase H3K36me2 at DNA damage sites to inhibit transcription and promote repair. *Aging (Albany NY)* 12: 11165–11184

Rezazadeh S, Yang D, Tombline G, Simon M, Regan SP, Seluanov A, Gorbunova V (2019) SIRT6 promotes transcription of a subset of NRF2 targets by mono-ADP-ribosylating BAF170. *Nucleic Acids Res* 47: 7914–7928

Roichman A, Elhanati S, Aon MA, Abramovich I, Di Francesco A, Shahar Y, Avivi MY, Shurgi M, Rubinstein A, Wiesner Y *et al* (2021) Restoration of energy homeostasis by SIRT6 extends healthy lifespan. *Nat Commun* 12: 3208

Roichman A, Kanfi Y, Glazz R, Naiman S, Amit U, Landa N, Tinman S, Stein I, Pikarsky E, Leor J *et al* (2017) SIRT6 overexpression improves various aspects of mouse healthspan. *J Gerontol A Biol Sci Med Sci* 72: 603–615

Ryu S, Han J, Norden-Krichmar TM, Schork NJ, Suh Y (2018) Effective discovery of rare variants by pooled target capture sequencing: a comparative analysis with individually indexed target capture sequencing. *Mutat Res* 809: 24–31

Schuster S, Roessler C, Meleshin M, Zimmermann P, Simic Z, Kambach C, Schiene-Fischer C, Steegborn C, Hottiger MO, Schutkowski M (2016) A continuous sirtuin activity assay without any coupling to enzymatic or chemical reactions. *Sci Rep* 6: 22643

Sebastian C, Zwaans BM, Silberman DM, Gymrek M, Goren A, Zhong L, Ram O, Truelove J, Guimaraes AR, Toiber D *et al* (2012) The histone deacetylase SIRT6 is a tumor suppressor that controls cancer metabolism. *Cell* 151: 1185–1199

Seluanov A, Mao Z, Gorbunova V (2010) Analysis of DNA double-strand break (DSB) repair in mammalian cells. *J Vis Exp* 43: 2002

Shechter D, Dormann HL, Allis CD, Hake SB (2007) Extraction, purification and analysis of histones. *Nat Protoc* 2: 1445–1457

Sidoli S, Bhanu NV, Karch KR, Wang X, Garcia BA (2016) Complete workflow for analysis of histone post-translational modifications using bottom-up mass spectrometry: from histone extraction to data analysis. *J Vis Exp* 111: 54112

Sidoli S, Kori Y, Lopes M, Yuan ZF, Kim HJ, Kulej K, Janssen KA, Agosto LM, Cunha J, Andrews AJ *et al* (2019) One minute analysis of 200 histone posttranslational modifications by direct injection mass spectrometry. *Genome Res* 29: 978–987

Sidoli S, Lin S, Xiong L, Bhanu NV, Karch KR, Johansen E, Hunter C, Mollah S, Garcia BA (2015) Sequential window acquisition of all theoretical mass

spectra (SWATH) analysis for characterization and quantification of histone post-translational modifications. *Mol Cell Proteomics* 14: 2420–2428

Simon M, Van Meter M, Ablaeva J, Ke Z, Gonzalez RS, Taguchi T, De Cecco M, Leonova KI, Kogan V, Helfand SL *et al* (2019) LINE1 derepression in aged wild-type and SIRT6-deficient mice drives inflammation. *Cell Metab* 29: 871–885

Tasselli L, Xi Y, Zheng W, Tennen RI, Odrowaz Z, Simeoni F, Li W, Chua KF (2016) SIRT6 deacetylates H3K18ac at pericentric chromatin to prevent mitotic errors and cellular senescence. *Nat Struct Mol Biol* 23: 434–440

TenNapel MJ, Lynch CF, Burns TL, Wallace R, Smith BJ, Button A, Domann FE (2014) SIRT6 minor allele genotype is associated with >5-year decrease in lifespan in an aged cohort. *PLoS One* 9: e115616

Tian X, Firsanov D, Zhang Z, Cheng Y, Luo L, Tombline G, Tan R, Simon M, Henderson S, Steffan J *et al* (2019) SIRT6 is responsible for more efficient DNA double-strand break repair in long-lived species. *Cell* 177: 622–638

Van Meter M, Kashyap M, Rezazadeh S, Geneva AJ, Morello TD, Seluanov A, Gorbunova V (2014) SIRT6 represses LINE1 retrotransposons by ribosylating KAP1 but this repression fails with stress and age. *Nat Commun* 5: 5011

Van Meter M, Mao Z, Gorbunova V, Seluanov A (2011) SIRT6 overexpression induces massive apoptosis in cancer cells but not in normal cells. *Cell Cycle* 10: 3153–3158

Van Meter M, Simon M, Tombline G, May A, Morello TD, Hubbard BP, Bredbenner K, Park R, Sinclair DA, Bohr VA *et al* (2016) JNK phosphorylates SIRT6 to stimulate DNA double-strand break repair in response to oxidative stress by recruiting PARP1 to DNA breaks. *Cell Rep* 16: 2641–2650

Vivelo CA, Wat R, Agrawal C, Tee HY, Leung AK (2017) ADPriboDB: the database of ADP-ribosylated proteins. *Nucleic Acids Res* 45: D204–D209

Vohhodina J, Barros EM, Savage AL, Liberante FG, Manti L, Bankhead P, Cosgrove N, Madden AF, Harkin DP, Savage KI (2017) The RNA processing factors THRAP3 and BCLAF1 promote the DNA damage response through selective mRNA splicing and nuclear export. *Nucleic Acids Res* 45: 12816–12833

Wisniewski JR (2017) Label-free and standard-free absolute quantitative proteomics using the "total protein" and "proteomic ruler" approaches. *Methods Enzymol* 585: 49–60

Zhang W, Wan H, Feng G, Qu J, Wang J, Jing Y, Ren R, Liu Z, Zhang L, Chen Z *et al* (2018) SIRT6 deficiency results in developmental retardation in cynomolgus monkeys. *Nature* 560: 661–665

Zullo JM, Demarco IA, Pique-Regi R, Gaffney DJ, Epstein CB, Spooner CJ, Luperchio TR, Bernstein BE, Pritchard JK, Reddy KL *et al* (2012) DNA sequence-dependent compartmentalization and silencing of chromatin at the nuclear lamina. *Cell* 149: 1474–1487